Geomorphology 284 (2017) 156–174

Contents lists available at ScienceDirect

Geomorphology

journal homepage: www.elsevier.com/locate/geomorph

Quaternary history and landscape evolution of a high-altitude intermountain basin at the western end of the Himalayan-Tibetan orogen, Waqia Valley, Chinese Pamir

Kathryn A. Hedrick [a], Lewis A. Owen [a,*], Jie Chen [b], Alex Robinson [c], Zhaode Yuan [d], Xiaodong Yang [b], Daniel B. Imrecke [c,e], Wenqiao Li [b], Marc W. Caffee [f,g], Lindsay M. Schoenbohm [h], Boxuan Zhang [b]

[a] Department of Geology, University of Cincinnati, Cincinnati, OH 45221, USA
[b] State Key Laboratory of Earthquake Dynamics, Institute of Geology, China Earthquake Administration, Beijing 100029, China
[c] Department of Earth and Atmospheric Sciences, University of Houston, Houston, TX 77004, USA
[d] China Earthquake Disaster Prevention Center, Beijing 100029, China
[e] Division of Natural Sciences, University of Houston – Clear Lake, Houston, TX 77058, USA
[f] Department of Physics and Astronomy, Purdue University, West Lafayette, IN 47907, USA
[g] Department of Earth, Atmospheric, and Planetary Sciences, Purdue University, West Lafayette, IN 47907, USA
[h] Department of Earth Sciences, University of Toronto, Toronto, ON, 55S 3B1, Canada

ARTICLE INFO

Article history:
Received 24 February 2016
Received in revised form 26 August 2016
Accepted 1 September 2016
Available online 3 September 2016

Keywords:
Terrestrial cosmogenic nuclide dating
Glaciation
Alluvial fans
River terraces
Valley fills
Climate change
Tectonics
Erosion rates

ABSTRACT

Quaternary valley fills and landforms in the Waqia valley of the Chinese Pamir were examined using geomorphic mapping, geomorphic and sedimentological analysis of landforms and sediments, and cosmogenic ^{10}Be surface exposure dating. Six sets of moraines (M-1 to M-6) are identified and date to the penultimate or an older glacial cycle (M-1), penultimate glacial cycle (M-2), early last glacial and probably Marine Oxygen Isotope Stage (MIS) 4 (M-3), MIS 2 (M-4), Late Glacial (M-5), and early Holocene (M-6). Younger moraines are also present, but these were not examined in detail. Alluvial fans and outwash/river terraces are present throughout the valley. Four surfaces on alluvial fans and river terraces were dated to ~580 ka (T-1), ~120 ka (T-2), ~100 ka (T-3), and ~70 ka (T-4). Large landslide and lacustrine deposits are common within the valley fills and represent periods of major slope instability and possible damming of drainages. Glacial processes dominate the western side of the valley; landsliding is the leading process on its eastern side. Defining the nature and timing of landform formation in this valley highlights the punctuated nature of landform evolution in the Himalaya and Tibet and provides a framework for considering the abundant valley fill successions elsewhere in the orogen.

1. Introduction

Impressive Quaternary valley fills are present throughout the Himalayan-Tibetan orogen, providing a geomorphic and sedimentary archive of paleoenvironmental change and landscape development (Owen, 1989; Owen and Derbyshire, 1993; Barnard et al., 2006; Seong et al., 2009b; Blöthe et al., 2014; Scherler et al., 2014). The Waqia valley in the Chinese Pamir contains one of the most extraordinary Quaternary valley fill successions within the Himalayan-Tibetan orogen, comprising successions of glacial, fluvial, lacustrine, and landslide sediments that are hundreds of meters thick, with landforms that include moraines, alluvial fans, and river terraces, many of which are highly dissected and deformed. We undertook a study of the valley fill deposits and landforms in the Waqia valley as part of a long-term effort to understand the Quaternary evolution of the Chinese Pamir (Robinson et al., 2007: Robinson, 2009; Owen et al., 2012; Yuan et al., 2013). In particular, we focused on the relationship between glaciation, and alluvial fan and river terrace development utilizing field mapping, remote sensing, sedimentological and geomorphic methods, and cosmogenic ^{10}Be surface exposure dating.

Our study provides a framework for future geomorphic, sedimentary, tectonic, and Quaternary research of the abundant valley fill successions that exist throughout the Himalayan-Tibetan orogen. This study also highlights the potential for preserving long records of paleoenvironmental change and landscape evolution within valleys in the Himalayan-Tibetan orogen. Many of these are important archives for Quaternary paleoenvironmental change and landscape evolution, but their potential has yet to be fully appreciated and utilized.

2. Regional setting

The Waqia valley is located in the Chinese Pamir in Xinjiang Province, western China, near the borders of Pakistan, Afghanistan, and Tajikistan (Fig. 1). The valley stretches NW-SE for ~50 km at the interpreted northern end of the Karakax fault system, which is the

* Corresponding author.
E-mail address: Lewis.Owen@uc.edu (L.A. Owen).

http://dx.doi.org/10.1016/j.geomorph.2016.09.002
0169-555X/

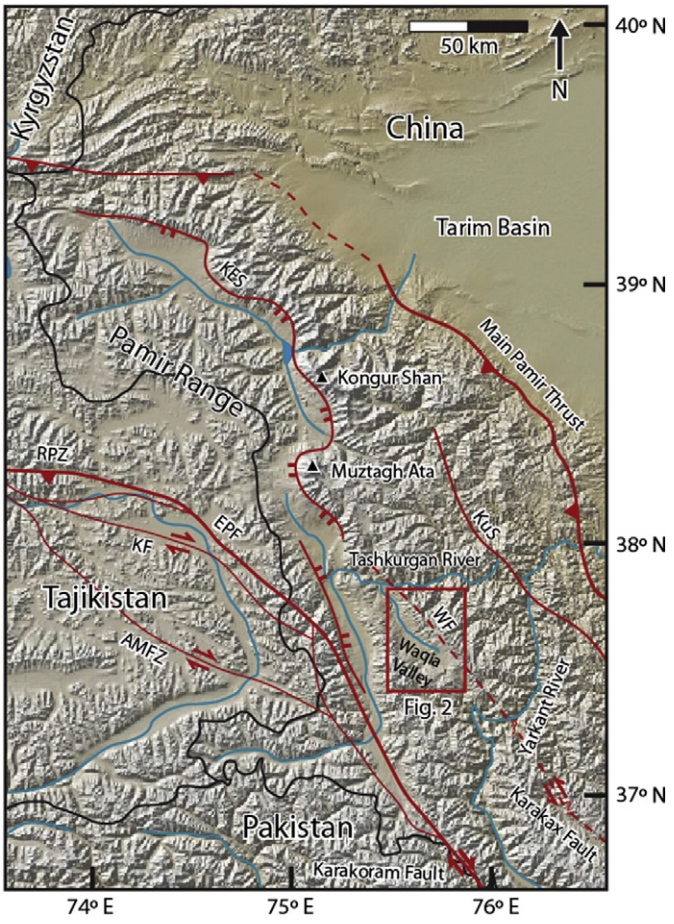

Fig. 1. Digital elevation models (GMRT accessed through GeoMapApp) showing study area (red rectangle) in the Pamir with locations of major faults (red lines, from Robinson et al., 2004). Country borders are shown in black, and rivers and lakes in blue. WF: Waqia Fault, KES: Kongur Extensional System, RPZ: Rushan Pshart Zone, EPF: East Pamir Fault, KF: Karasu Fault, AMFZ: Aksu-Murgab Fault Zone, KuS: Kunlun Suture.

western continuation of the Altyn Tagh fault (Brunel et al., 1994; Robinson et al., 2007). The NW flowing Waqia River, which drains the valley, flows into the Tashkurgan and then the Yarkand rivers, which empty into the Tarim Basin. The valley floor rises from ~2900 m above sea level (asl) to peaks that exceed 5000 m asl. The climate is semiarid; no meteorological stations exist in valley, but meteorological data available in the town of Tashkurgan, ~20 km to the west of the valley, show a mean annual precipitation of 68 mm for the period between 1971 and 2000, with 65% of the precipitation falling in May through August, with the July and January average high temperatures being 23.7 and −18.6 °C, respectively (Weather China, 2012, cited in Owen et al., 2012). Vegetation is of the desert-steppic type along the valley floors, transitioning to alpine type at higher elevations.

No previous Quaternary geologic studies have been undertaken in the Waqia valley, but several studies on the glacial geology and Quaternary landsliding have been undertaken in the Tashkurgan valley that is ~20 km to the west (Fig. 1: Fort and Peulvast, 1995; Owen et al., 2012; Xu et al., 2013; Yuan et al., 2013). Owen et al. (2012) documented previous glacial advances into the Tashkurgan valley and defined four glacial stages: (i) the Dabudaer glacial stage that dates to the penultimate glacial cycle and/or earlier, and may represent one or more glaciations; (ii) the Tashkurgan glacial stage that dates to early last glacial, most probably Marine Oxygen Isotope Stage (MIS) 4; (iii) the Hangdi glacial stage that dates to MIS 2, possibly early MIS 2; and (iv) the Kuzigun glacial stage that dates to MIS 2, possibly the global last glacial maximum, and is younger than the Hangdi glacial stage. Owen et al. (2012) also noted that younger moraines and rock glaciers are present at the heads of tributary valleys, but they were not able to date these landforms.

3. Methods

3.1. Mapping

Geomorphic surfaces and landforms were identified and mapped in the field with the aid of *Google Earth* imagery (Fig. 2). The extent of alluvial fan and fluvial terraces, active channels, loess, and moraines and glacial deposits were mapped on the basis of morphostratigraphy, considering their geomorphic context and relative weathering characteristics, utilizing the morpho-, litho- and allostratigraphic approaches highlighted by Hughes (2010). Glacial landforms were numbered based on their relative ages, M-1 (oldest) through M-6 (youngest). Similarly, alluvial fan and terraces were numbered based on their relative ages, T-1 (oldest) through T-4 (youngest). Landforms and sedimentary deposits were examined using the methods summarized in Benn and Owen (2002). Many studies have highlighted the confusion surrounding the misidentification of glacial and nonglacial landforms and diamicts in the Himalaya and Tibet (Derbyshire, 1983; Owen, 1991; Hewitt, 1999; Benn and Owen, 2002; Seong et al., 2009a, 2009b). In particular, large landslides can easily be mistaken for moraines and vice versa. In an extreme case this has contributed to the erroneous reconstruction of an ice sheet over Tibet and adjacent Himalaya (see page 19 of Owen and Dortch, 2014 for a fuller discussion). We recognize this problem and use the criteria in Owen (1991), Hewitt (1999), and Benn and Owen (2002) to address this issue.

3.2. ^{10}Be dating and analysis

Samples were collected from several of the most representative glacial, alluvial fan, and fluvial landforms for each relative age. Glacial deposits included terminal (M-6), lateral (M-5), and hummocky moraines (M-2 to M-4) and a glaciofluvial outwash plain (T-4). The oldest moraine (M-1) was highly eroded into discontinuous patches.

Where available, well-defined and sharp-crested moraine ridges were sampled (e.g., M-3); well-defined moraine ridges were not common on many hummocky moraines or well-worn glacial surfaces. For hummocky moraines, sampled boulders were located preferentially on the highest available ridges away from slopes and depressions (M-4, M-5, and M-6). Boulder samples collected from glaciofluvial terraces and alluvial fans were taken from boulders located on well-defined fluvial bars or flat alluvial fan surfaces to reduce the likelihood of sampling boulders significantly affected by sediment shielding.

We preferentially selected quartz-rich boulders for ^{10}Be dating that were: (i) large, >50 cm in length (a-axis) and generally 1–7 m across for moraines and 0.5–0.8 m for alluvial fan/terraces; and (ii) tall in height relative to the surrounding land surface (>50 cm exposed) to avoid boulder surfaces that may have been recently shielded by sediment or that could be shielded by snow. Where large boulders were not available, boulders with the best placement and the largest size were sampled (Table 1). Preferred boulders were also embedded into the moraines, indicating that they retained their original placement and showed no sign of toppling. Additionally, boulders that had a well-developed rock varnish and maintained a hard, resistant surface were favored to try to avoid surfaces that may have experienced significant weathering. Boulder characteristics are recorded in Table 1. We took ~500 g of sample from a high, flat surface on each sampled boulder to a depth of 1–5 cm using a small sledgehammer and chisel. Topographic shielding was determined by use of inclinometer, taking angle measurements from the sample to the horizon in 10° increments.

Two-meter-deep pits were dug into alluvial fan and river terraces (T-1, T-2, and T-3) to collect samples for ^{10}Be depth profile analysis.

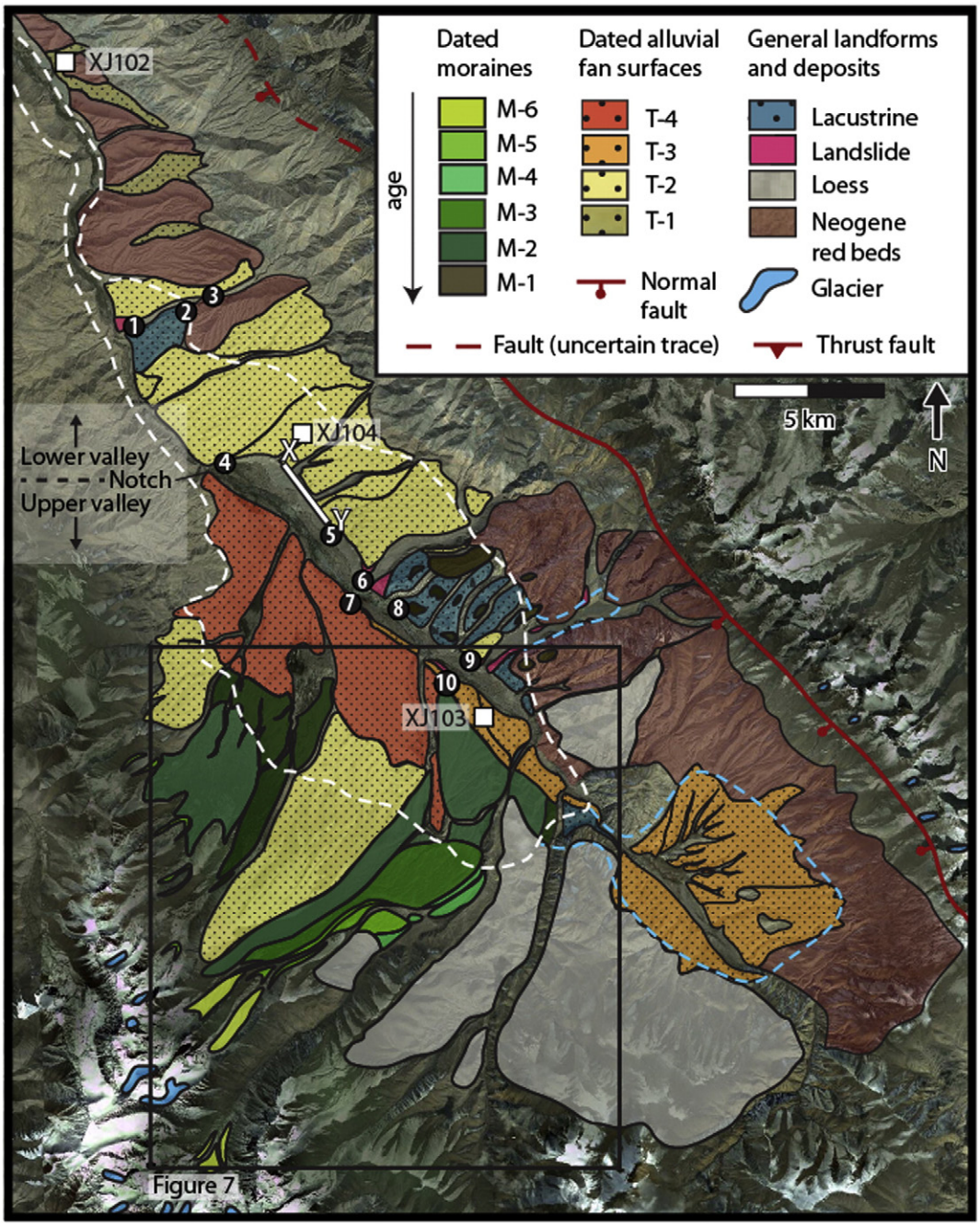

Fig. 2. Overview of study area (location shown by red rectangle in Fig. 1) showing locations of major fault and important landforms including dated surfaces (M-1–M-6; T-1–T-4) and mapped deposits and landforms plotted on Google Earth imagery. White dashed line indicates the boundaries of the proposed Waqia Paleolake. Blue dashed line outlines a former ice dammed lake blocked during M-1 and M-2. Black circles with white text indicate important locations mentioned in the text and their associated figures. (1) Landslide deposits (Section 4.2 of this paper; Fig. 6). (2) Location of ice-rafted debris in deformed lacustrine sediments (Section 4.1). (3) Soft-sediment deformation and rip-up clasts in clay (Section 4.1). 4) Shoreline notches (Section 4.1). (5) Modern bajada (Section 4). (6) Landslide deposits (Section 4.2). (7) Landslide deposits (Section 4.2). (8) Complex sedimentary sequence comprising interbedded deformed lacustrine silts and diamicts (Section 4). (9) Landslide deposits (Section 4.2). (10) Dropstones in lacustrine clays with lenses of fine sand (section 4.1). The small white squares show the locations of the ^{10}Be depth profiles.

We collected ~1 kg of quartz pebbles (3–5 cm in diameter) at intervals of 30–50 cm each with at least four samples per pit (Table 2); the shallow samples at 40 cm (T-1), 20 cm (T-2), and 30 cm (T-3) depths did not yield enough quartz for ^{10}Be measurement.

Samples were processed at the Geochronology Laboratories at the University of Cincinnati. Each boulder sample was crushed and sieved to obtain the 250–500 μm grain size fraction. For depth profiles, 500 g of amalgamated quartz pebbles were crushed and sieved to obtain the 250–500 μm grain size fraction. Quartz isolation, dissolution, chromatography, isolation of Be, and preparation of BeO followed the methods of Kohl and Nishiizumi (1992) for all samples; these methods are described in detail in Dortch et al. (2009). The ^{10}Be/^{9}Be were measured using accelerator mass spectrometry at the Purdue Rare Isotope Measurement Laboratory at Purdue University. The ^{10}Be exposure ages were calculated using the CRONUS age calculator (version 2.2, Balco et al., 2008; Table 1).

Cosmogenic nuclide depth profile results were calculated using Hidy et al.'s (2010) MATLAB-based Monte Carlo simulator (version 1.2), which produces best-fit depth profile curves and provides estimates of erosion rate and inheritance. For these simulations we use a reference

Table 1
Sample boulder locations and characteristics for terrestrial cosmogenic nuclide surface age dating for moraines and glaciofluvial outwash plains and ^{10}Be age results.

Sample	Glacial landforms or terrace	Latitude (°N)	Longitude (°E)	Altitude (m asl)	Boulder size height/width/length (cm)	Sample lithology	Quartz mass (g)	Be carrier (g)	Be carrier concentration (mg/g)	^{10}Be/^{9}Be (10^{-13})	Sample thickness (cm)	^{10}Be concentration (atom/g SiO_2 $SiO2 \times 10^5$)[a]	Lal (1991), Stone (2000) time-independent age (ka)[a, b]	Desilets and Zreda (2006) age (ka)[a, b]	Dunai (2000) age (ka)[a, b]	Lifton et al. (2005) age (ka)[a, b]	Lifton et al. (2014) flux time dependent age (ka)[a, b, c]	Lal (1991), Stone (2000) time-dependent age (ka)[a, b]
Pamir48	M-1	37.5983	75.6710	3662	240/140/110	Chert	21.2264	0.3512	1.354	28.3 ± 2.63	2	42.40 ± 3.94	86.4 ± 11.2	72.6 ± 1.1	71.1 ± 10.8	69.5 ± 9.6	85.0 ± 11.0	78.5 ± 10.0
Pamir51	(moraine)	37.5979	75.6709	3663	150/100/60	Chert	20.5225	0.3511	1.354	11.45 ± 3.26	4	17.73 ± 5.05	35.6 ± 3.3	31.5 ± 3.7	31.2 ± 3.8	30.5 ± 3.1	36.7 ± 2.8	33.3 ± 3.0
XJ98	M-2	37.5218	75.5780	4437	250/210/70	Metagranite	25.4376	0.358	1.414	47.5 ± 2.00	2.5	60.72 ± 2.66	82.6 ± 8.2	65.4 ± 8.4	63.8 ± 8.1	62.5 ± 6.9	78.5 ± 8.2	74.8 ± 7.2
XJ99	(moraine)	37.5212	75.5692	4619	290/180/70	Metagranite	18.4017	0.3452	1.414	30.2 ± 0.52	2	53.56 ± 0.92	66.2 ± 6.0	51.2 ± 6.2	49.7 ± 6.0	48.5 ± 4.9	62.0 ± 5.0	60.2 ± 5.3
XJ100		37.5210	75.5705	4632	250/210/80	Metagranite	23.2395	0.3618	1.414	24.6 ± 0.63	2	36.21 ± 0.92	44.24 ± 4.05	35.66 ± 4.34	34.95 ± 4.24	34.4 ± 3.5	42.0 ± 3.0	40.1 ± 3.6
XJ108	T-4 (glaciofluvial	37.5890	75.6286	3483	45/35/30	Quartz	16.5806	0.3569	1.414	30.5 ± 0.60	2.5	61.94 ± 1.21	140.3 ± 12.9	116.2 ± 14.3	113.7 ± 13.9	111.3 ± 11.5	136 ± 13	124.1 ± 11.0
XJ109	outwash	37.5906	75.6309	3483	80/50/38	Granite	25.7435	0.3509	1.354	30.7 ± 0.89	3.5	33.16 ± 0.96	73.4 ± 6.8	63.0 ± 7.8	61.0 ± 7.6	60.4 ± 6.3	73.2 ± 6.8	66.9 ± 6.1
XJ110	plain)	37.5906	75.6318	3479	60/50/20	Granite	17.818	0.3552	1.414	15.5 ± 0.48	2.5	29.19 ± 0.91	65.0 ± 6.1	55.9 ± 6.9	54.8 ± 6.8	53.2 ± 5.6	65.0 ± 5.4	59.5 ± 5.4
XJ90	M-3	37.5313	75.6285	3970	310/220/150	Metagranite	24.3242	0.3617	1.414	26.9 ± 0.90	3	37.79 ± 1.26	65.0 ± 6.2	53.4 ± 6.6	52.2 ± 6.5	50.6 ± 5.3	63.4 ± 5.3	59.3 ± 5.5
XJ91	(moraine)	37.5339	75.6303	3952	175/80/100	Granodiorite	27.5307	0.3574	1.414	8.14 ± 0.32	3	9.98 ± 0.40	17.1 ± 1.6	16.2 ± 2.0	16.4 ± 2.0	15.8 ± 1.7	19.5 ± 1.4	16.9 ± 1.6
XJ92		37.5355	75.6321	3938	210/155/100	Diorite	21.7623	0.341	1.354	5.45 ± 0.15	4	7.73 ± 0.21	13.5 ± 1.2	13.1 ± 1.6	13.4 ± 1.6	12.8 ± 1.3	15.9 ± 1.3	13.5 ± 1.2
XJ93		37.5339	75.6384	3865	140/120/60	Granodiorite	24.9633	0.3558	1.354	17.4 ± 0.29	2.5	22.48 ± 0.38	40.5 ± 3.6	34.8 ± 4.2	34.4 ± 4.1	33.7 ± 3.4	40.2 ± 2.8	37.3 ± 3.2
XJ94		37.5353	75.6415	3843	320/145/150	Metagranite	18.67	0.3557	1.414	16.9 ± 1.38	4	30.41 ± 2.48	56.3 ± 6.8	46.4 ± 6.7	45.6 ± 6.6	44.3 ± 5.7	55.6 ± 6.7	50.7 ± 6.0
XJ95		37.5342	75.6418	3847	280/250/110	Granite	27.8628	0.3756	1.354	25.9 ± 0.68	5	31.56 ± 0.83	58.8 ± 5.4	48.4 ± 5.9	47.5 ± 5.8	46.2 ± 4.8	58.2 ± 5.2	53.2 ± 4.8
XJ96		37.5328	75.6427	3866	160/130/60	Diorite	23.3843	0.3374	1.414	8.73 ± 0.35	2.5	11.90 ± 0.48	21.3 ± 2.1	19.8 ± 2.5	19.9 ± 2.5	19.2 ± 2.1	23.3 ± 1.9	20.8 ± 2.0
XJ97		37.5293	75.6372	3884	220/130/70	Metagranite	18.7403	0.3509	1.414	17.7 ± 0.67	4	31.36 ± 1.19	26.8 ± 5.5	46.6 ± 5.8	45.8 ± 5.7	44.6 ± 4.8	56.0 ± 5.4	51.2 ± 4.8
XJ5	M-4	37.5274	75.6459	3715	115/85/40	Metagranite	18.4684	0.3625	1.4140	4.19 ± 0.22	3	7.76 ± 0.40	15.1 ± 1.5	14.7 ± 1.9	15.0 ± 1.9	14.4 ± 1.6	17.7 ± 1.5	15.0 ± 1.5
XJ6	(moraine)	37.5281	75.6454	3735	100/180/50	Metagranite	18.7528	0.3491	1.3540	9.77 ± 0.29	4	16.46 ± 0.49	32.1 ± 3.0	28.7 ± 3.5	28.4 ± 3.5	27.8 ± 2.9	33.3 ± 2.6	30.3 ± 2.7
XJ7		37.5272	75.6452	3738	180/120/65	Metagranite	17.6766	0.3598	1.3540	4.20 ± 0.17	4	7.73 ± 0.32	15.0 ± 1.5	14.6 ± 1.8	14.9 ± 1.9	14.3 ± 1.5	17.6 ± 1.4	14.9 ± 1.4
XJ10		37.5247	75.6418	3760	720/300/190	Metagranite	15.3721	0.3392	1.3540	5.90 ± 0.34	1	11.78 ± 0.67	22.0 ± 2.3	20.5 ± 2.7	20.6 ± 2.7	20.0 ± 2.3	24.1 ± 2.11	21.4 ± 2.2
XJ12	M-5	37.5253	75.6123	4137	120/80/35	Metagranite	17.7061	0.3582	1.3540	3.73 ± 0.17	5	6.82 ± 0.32	10.8 ± 1.1	10.6 ± 1.3	11.0 ± 1.4	10.3 ± 1.1	13.0 ± 1.2	10.8 ± 1.0
XJ13	(moraine)	37.5255	75.6110	4136	130/85/35	Metagranite	18.4126	0.3556	1.354	2.90 ± 0.13	5	5.06 ± 2.24	8.0 ± 3.6	8.1 ± 3.7	8.5 ± 2.9	7.9 ± 3.6	9.8 ± 4.6	8.0 ± 3.6
XJ14		37.5246	75.6102	4152	200/85/75	Gneiss	15.9137	0.3658	1.3540	4.53 ± 0.17	5	9.41 ± 0.36	14.8 ± 1.4	14.1 ± 1.8	14.4 ± 1.8	13.7 ± 1.5	17.2 ± 1.4	14.8 ± 1.4
XJ15		37.5250	75.6095	4153	330/160/75	Gneiss	16.4844	0.3637	1.3540	4.81 ± 0.12	3	9.60 ± 0.24	14.9 ± 1.4	14.1 ± 1.7	14.4 ± 1.7	13.8 ± 1.4	17.2 ± 1.3	14.8 ± 1.3
XJ16		37.5239	75.6074	4176	230/105/75	Gneiss	23.8605	0.3446	1.3540	4.05 ± 0.11	5	5.29 ± 0.15	8.1 ± 0.8	8.2 ± 1.0	8.6 ± 1.1	8.0 ± 0.8	10.0 ± 0.9	8.2 ± 0.7
Pamir36	M-6	37.4561	75.5594	4555	240/180/50	Quartzite	18.9892	0.3507	1.354	3.57 ± 0.38	4	5.96 ± 0.51	7.6 ± 0.9	7.5 ± 1.1	7.9 ± 1.2	7.3 ± 1.0	9.2 ± 1.2	7.6 ± 0.9
Pamir37	(moraine)	37.4560	75.5598	4556	130/130/40	Quartzite	20.8433	0.3502	1.354	0.76 ± 0.07	2	1.2 ± 0.1	1.5 ± 0.2	1.5 ± 0.2	1.6 ± 0.3	1.4 ± 0.2	1.89 ± 0.28	1.5 ± 0.2
Pamir38		37.4555	75.5595	4572	180/120/60	Quartzite	16.5853	0.3502	1.354	4.81 ± 0.30	3	9.2 ± 0.6	11.6 ± 1.2	1.1 ± 1.5	1.1 ± 1.5	1.1 ± 1.3	13.7 ± 1.3	11.6 ± 1.2
Pamir39		37.4558	75.5597	4567	130/130/40	Quartzite	24.1526	0.3507	1.354	6.32 ± 1.41	2.5	8.3 ± 1.9	10.4 ± 2.5	10.0 ± 2.5	1.0 ± 2.6	9.8 ± 2.4	12.4 ± 2.7	10.4 ± 2.5

[a] Reported uncertainty is expressed as 1σ.
[b] Ages determined using a rock density of 2.75 g/cm^3 and 07KNSTD standard. Uncertainties include analytical and production rate/scale model uncertainties. Only sample Pamir48 required a correction for shielding (0.998).
[c] Ages calculated using CRONUS calculator at http://web1.ittc.ku.edu:8888/2.0/.

Table 2
Terrestrial cosmogenic nuclide depth profile and ^{10}Be measurement results for alluvial fans surfaces T-1, T-2, and T-3[a].

Terrace name	Latitude/longitude and altitude (m asl)	Sample name	Sample depth (cm)	Quartz mass (g)	Be carrier mass (g)[b]	^{10}Be/^{9}Be (10^{-13})[c]	^{10}Be concentration (atom/g SiO_2 $SiO_2 \times 10^5$)[b]	Inheritance[d] (10^4 atoms/g)	Erosion rate[d] (m/Ma)	Age[d] (ka)
T-1	37.7794°N/75.5060°E 3084	XJ102	*70 ± 5*	*24.0798*	*0.3500*	*31.19 ± 0.30*	*41.02 ± 0.40*	**58.26**	**0.10**	**581.5**
			100 ± 5	23.0351	0.3503	32.52 ± 0.57	44.75 ± 0.78	21.3–77.3	0.01–0.12	463.2–903.6
			130 ± 5	23.1138	0.3508	23.66 ± 0.50	32.49 ± 0.69			
			160 ± 5	23.5775	0.3500	17.19 ± 0.24	23.08 ± 0.32			
			190 ± 5	23.3271	0.3502	12.53 ± 0.21	17.02 ± 0.28			
T-2	37.6682°N/75.5909°E 3439	XJ104	50 ± 5	23.9445	0.3502	19.34 ± 0.36	25.60 ± 0.47	**39.13**	**0.43**	**120.7**
			80 ± 5	24.2886	0.3509	12.54 ± 0.27	16.39 ± 0.35	11.06–54.79	0.04–0.50	103.4–208.1
			120 ± 5	24.4163	0.3507	8.65 ± 0.25	11.12 ± 0.32			
			150 ± 5	*25.3371*	*0.3507*	*10.10 ± 0.17*	*12.63 ± 0.32*			
			190 ± 5	*23.1432*	*0.3510*	*7.88 ± 0.22*	*10.82 ± 0.30*			
T-3	37.5796°N/75.6666°E 3471	XJ103	60 ± 5	25.7478	0.3516	14.68 ± 0.20	18.13 ± 0.24	**19.29**	**0.54**	**97.1**
			90 ± 5	25.7410	0.3508	9.66 ± 0.16	11.91 ± 0.20	11.34–24.29	0.05–0.66	81.6–161.6
			120 ± 5	22.0591	0.3505	6.43 ± 0.10	9.24 ± 0.14			
			150 ± 5	23.0346	0.3503	4.46 ± 0.204	6.14 ± 0.28			
			190 ± 5	22.1476	0.3515	3.15 ± 0.08	4.53 ± 0.11			

[a] Italicized samples are outliers and were removed from the final data set for Monte Carlo simulation.
[b] All samples were processed using 1.354 ppm ^{9}Be carrier.
[c] Reported uncertainty is expressed as 1σ.
[d] Bayesian most probable values (bold) and 2 σ upper and lower inheritance, erosion rate, or age range as determined by Monte Carlo simulation.

production rate of 4.39 atoms g^{-1} y^{-1} with 5% error in ^{10}Be half-life, adjusted for the sampling site latitude and elevation using Lal's (1991) and Stone's (2000) time-dependent scaling scheme. The shielding value for all depth profiles was set at 1, as all depth profile pits were located far from mountain fronts and other high-relief features, which might have affected cosmogenic ray exposure. Because of sample scatter, calculating depth profile curves with confidence levels of 1σ (XJ-102), 3σ (XJ-103), and 2σ (XJ-104) was necessary, and outliers were removed from the XJ-102 and XJ-104 sample sets (Table 2). For the T-1 depth profile (XJ-102), the shallowest sample (~70 cm) was removed from the simulation as an outlier to obtain a best-fit curve. We suggest that the low ^{10}Be concentration is a result of disturbance of the sediment layer because of bioturbation. Cover was also assigned at a value of 1; this decision was made because the fact that each surface sampled by depth profile illustrated evidence of variable loess cover through time, e.g., multiple loess soils within a pit, patchy loess cover on sampled surfaces, and by assigning a value that assumes no cover we hope to avoid including additional, unknown uncertainty because of fluctuating loess cover of undefined thickness through time to the simulator results. The density of the alluvial fan deposits was not directly measured due to logistical difficulties. We assume a stochastic uniform sediment density at depth within the range of 2.0 and 2.7 g cm^{-2} for all depth profiles. Although density approaching 2.7 g cm^{-2} may seem high, the alluvial fan deposits of XJ-103 are composed primarily of large, quartz-rich boulders, and were relatively well consolidated, and therefore approach the density of solid rock. The XJ-102 and XJ-104 deposits are composed of much finer material, densely packed. Additionally, density in these profiles may have changed over time because such factors as the production of soil and variable loess cover. This density range is comparable to that measured by other researchers (e.g., Braucher et al., 2011; Rodés et al., 2011) in alluvial fan deposits with similar characteristics.

Two sets of problems are associated with the application of cosmogenic methods to date moraines in the Himalaya, Tibet and elsewhere, and are discussed in detail in numerous studies (e.g., Hallet and Putkonen, 1994; Aoki and Imamura, 1999; Schäfer, 2000; Benn and Owen, 2002; Brown et al., 2002; Owen et al., 2002, 2003a, b, 2005, 2006a, b, 2008, 2009, 2010, 2012; Putkonen and Swanson, 2003; Putkonen and O'Neal, 2006; Seong et al., 2007, 2009a; Putkonen et al., 2008; Dortch et al., 2010; Chevalier et al., 2011; Heyman et al., 2011; Owen and Dortch, 2014). The first set of problems relate to the use of the appropriate scaling models and geomagnetic corrections for ^{10}Be production to calculate ^{10}Be ages (e.g., Pigati and Lifton, 2004; Staiger et al., 2007; Owen and Dortch, 2014). Currently there is no consensus on the appropriate scaling model to be used for the Himalayan-Tibetan orogen, and there are no calibration sites in this region. To enable us to make comparison with most other studies in the region, e.g., such as summarized in Owen et al. (2012), Dortch et al. (2013), and Murari et al. (2014) and until a calibration site is established for the Himalaya and Tibet, we used the time-dependent model of Lal (1991)-Stone (2000; hereafter referred to as "Lal-Stone"). Age differences resulting from the various scaling systems calculated in CRONUS 2.2 are shown in detail in Table 1 for comparison. In addition, we recognize that the new scaling schemes such as those of Lifton et al. (2014) will produce ages that may be 5–20% older than the Lal-Stone time-constant model (Table 1). However, these differences in ages do not affect our stratigraphic or paleoclimatic conclusions. The second set of problems relates to geologic factors. These include weathering, exhumation, prior exposure, and shielding of the surface by snow and/or sediment. With the exception of prior exposure to cosmic rays, these factors generally reduce the concentration of cosmogenic nuclides in rock surfaces, producing underestimates of the true age of the landforms perhaps leading to a spread in apparent exposure ages on a landform. This is particularly so for moraines that are many hundreds of thousands of years old because their surface boulders generally are significantly weathered and/or may have been exhumed from depth during prolonged periods of erosion. Periods of prior exposure of boulders result in an overestimate of the true age of the moraine. Geologic factors often eclipse the problems associated with production rates. To help address the geologic problems, multiple samples are collected from the same surface, with the view that the variability of ages on the surface reflects the degree to which these factors have operated. Because these geologic factors are stochastic, little variability in ages reflects minimal geologic influence.

We examine our ^{10}Be exposure age results using normal distribution (mean and 1σ), probability density function (PDF), and mean square weighted deviation (MSWD) analysis to test the robustness of the data set and attempt to determine the most probable age for each surface. Comparison of data set mean and 1σ values gives a sense of data set scatter, whereas PDF analysis suggests the most likely age based on the range of age results. The MSWD analysis of results may elucidate the influence of geologic factors, e.g., erosion and inheritance, on the data set and give a sense of the usefulness of boulder ages as an isochron for surface age. Results for all statistical tests are shown in Table 3.

The uncertainty associated with accelerator mass spectrometry (AMS) measurements is given as 1σ values, which includes the internal (analytical) and external (analytical and production rate) uncertainty.

Table 3
Summary of boulder varnish and ages for all moraines and T-4 glaciofluvial outwash surface, and statistical analysis of surface ages. Moraines are correlated with Tashkurgan valley and SWHTS of Dortch et al. (2013).

Sample name	Surface name	Rock varnish	Time-dependent age[a] (ka)	Maximum age (ka)	Minimum age (ka)	2σ mean age (ka)	PDF age[b] (ka)	MSWD (ka)	Most likely age[c]
Pamir48	M-1	HV	33.3 ± 3.0	78.5 ± 10.0	33.3 ± 3.0	–	73.4	–	Penultimate glacial cycle or older
Pamir51		HV	78.5 ± 10.0						
XJ100	M-2	PV/LV	40.1 ± 3.6	74.8 ± 7.2	40.1 ± 3.6	58.4 ± 17.4	**60.0**	–	Penultimate glacial cycle
XJ99		PV/LV	60.2 ± 5.3				25.0–25.2		
XJ98		PV/LV	74.8 ± 7.2						
XJ108	T-4	LV	59.5 ± 5.4	124.1 ± 11.1	59.5 ± 5.4	63.2 ± 5.2	**68.0**	–	Early last glacial (MIS 4 and older)
XJ109		LV	66.9 ± 6.1				16.3–72.1		
XJ110		LV	*124.1 ± 11.1*						
XJ92	M-3	PV/LV	13.5 ± 1.2	20.8 ± 2.0	13.5 ± 1.2	17.0 ± 3.7	59.7	–	Early Last Glacial (MIS 4)
XJ91		PV/LV	16.9 ± 1.6						
XJ96		PV/NV	20.8 ± 2.0						
XJ93		PV/NV	37.3 ± 3.2	59.3 ± 5.5	37.3 ± 3.2	50.3 ± 8.1		53.5 ± 4.0	
XJ94		PV/NV	50.7 ± 6.0						
XJ97		PV/LV	51.2 ± 4.8						
XJ95		PV/NV	53.2 ± 4.8						
XJ90		PV/LV	59.3 ± 5.5						
XJ5	M-4	MV	14.9 ± 1.4	30.3 ± 2.7	14.9 ± 1.4	20.4 ± 7.3	**17.8**	–	MIS 2
XJ7		MV	15.0 ± 1.5				0–16.0		
XJ10		LV	21.4 ± 2.2						
XJ6		PV/HV	30.3 ± 2.7						
XJ13	M-5	PV/MV	8.0 ± 3.6	14.8 ± 1.3	8.0 ± 3.6	11.3 ± 3.3	**11.3**	–	Late Glacial
XJ16		NV	8.2 ± 0.7				5.6–7.4		
XJ12		PV/MV	10.8 ± 1.0						
XJ14		LV	14.8 ± 1.4						
XJ15		PV/LV	14.8 ± 1.3						
Pamir37	M-6	LV	*1.5 ± 0.2*	11.6 ± 1.2	1.5 ± 0.2	9.9 ± 2.1	10.4	–	Early Holocene
Pamir36		HV	7.6 ± 9.1						
Pamir39		HV	10.4 ± 2.5						
Pamir38		HV	11.6 ± 1.2						

– indicates no data/not applicable. HV = heavily varnished MV = moderately varnished LV = lightly varnished NV = no varnish PV = patchy varnish. Patchy varnish = typically lower sides of boulders are dark varnish, whereas upper (where sampled) is either no or lightly varnished.

[a] Italicized samples are 2σ outliers. Error shown in table is 1σ.

[b] All probability density function age values based off of ^{10}Be cobble/boulder data. Values in bold are the best estimates.

[c] Most likely age is determined by dating results within the context of the geomorphic landscape.

When using boulder age results to determine the possible age of a geomorphic surface, we utilized the mean and 2σ values; boulders that have ages outside 2σ are considered age outliers and are removed from the data set, and the mean age is calculated from the remaining samples. The uncertainties reported for the mean is 1σ of the nonoutlier sample population.

Evaluating sample ages using PDF allows determination of the most probable age of the surface based on the distribution of boulder ages. The PDF ages (Table 1) were calculated using a Matlab code (Jason Dortch, University of Manchester, *pers comm*., 2015).

The MSWD method of McDougall and Harrison (1999) aids in determining the existence of a statistically significant population of boulder ages and requires a population of three or more ages with an MSWD value <1 to be statistically significant. The MSWD values >1 suggest that scatter in boulder ages may be influenced more by geologic uncertainty than by analytical uncertainties (Powell et al., 2002), and the geologic context of the sampled boulders must be carefully considered. To calculate MSWD, McDougall and Harrison (1999) remove extreme outliers from the data set until a statistical indicator of $r^2 < 1$ has been reached (the sample population passes MSWD analysis) or the number of viable samples drops below three (the sample set fails MSWD analysis).

4. Geomorphology and sedimentology

The geomorphic character of the Waqia valley varies significantly downvalley (see Fig. 2). A bedrock notch present mid-valley marks a transition from the broad valley floor and floodplain of the upper valley to a narrower, incised channel in the lower valley segment. While the Quaternary deposits of the lower valley segment are dominated by thick, coarse alluvial fan deposits that overlie Neogene clastic basin deposits, the Quaternary deposits of the upper valley segment indicate operation of a more complex assortment of processes, including extensive gravitational, glacial, fluvial, lacustrine, and aeolian deposition, reworking, and erosion. Imrecke (2013) discusses the Neogene development of the basin in detail.

Lacustrine and alluvial fan deposits that are Neogene and Quaternary in age dominate the Waqia valley's eastern side. Impressive sedimentary sections are exposed along the central-eastern side of the Waqia valley stretching over 10 km and are in places >40 m high. The sections comprise a complex assemblage of diamictons, gravels, sands, and silts, which in places are deformed by soft-sediment deformation, faulted beds, and monoclinally folded lacustrine beds overlain unconformably by horizontal fluvial gravels. We refer to these sections as the central-eastern Waqia sections; they are described in detail below.

Glacial and glaciofluvial deposits are most common on the west side of the upper valley west of the main valley channel (Fig. 2), whereas glacial deposits are sparse on the east side. Evidence of glacial proximity east of the main valley channel includes dropstones ranging in size from pebbles to small boulders and other ice-rafted debris. Tilted bedding, overturned folds, load structures, and clastic dikes (discussed further in Section 4.2) present in many central-valley deposits may be indicators of glaciotectonism. Many of the moraines and glacial deposits within the main Waqia valley have been fluvially reworked and have deeply incised margins (M-2, M-3, M-4).

Most of the moraines in the upper Waqia valley (Fig. 2) are distinctive and range in character from relatively even, loess-covered surfaces (M-2) to gently undulating hummocky surfaces with small, incised channels (M-3 through M-5) and surfaces with deeper hummocks and significant signs of periglacial influence (M-6).

Conversely, the M-1 moraine comprises deposits of boulder-rich, silt-matrix deposits that are highly degraded; erosion has removed much of the M-1 material to leave several discrete clusters of boulders and silt diamict (located primarily between locations 8 and 9 shown in Fig. 2) at elevations ranging from 3450 to 3700 m asl. In some locations (e.g., tributary valley at location 9; Fig. 2) >1-m-long chert and granite boulders located on the valley floor with lithologies of both eastern and western range provenance are interpreted to originate from M-1 deposits. The largest glaciated valleys are concentrated in areas with catchments that face N to NE (M-1 through M-6 catchments and Fig. 2 tributary valley at location 1).

Loess cover is concentrated most significantly in the southernmost segment of the Waqia valley, where it is exposed in sections <2 m thick along road cuts, although the thickness of loess cover is still variable even within these zones. A thin (<30 cm) cap of loess is common on most moraine and alluvial fan deposits. Many of the geomorphically older alluvial fan surfaces located at higher elevations in the lower Waqia valley are covered in loess, which has developed a pervasive, semireddish-colored crust, reflecting formation of a biologic soil crust. Where investigated, this crust coincides with moderate soil development. The best developed crusts are observed on older alluvial fan surfaces in the lower Waqia valley (e.g. T-1; Fig. 2), whereas alluvial fan surfaces in the upper Waqia valley are characterized by the least developed crust (reddish coloration and hard texture restricted to a thin surface layer) where present (e.g. T-2; Fig. 2). This crust is notably absent on many surfaces, including moraine surfaces, in the upper Waqia valley. The ages and source of the loess in this region await further study.

The geomorphology of landforms juxtaposed across the main channel varies significantly from the NE to the SW side of the main valley. Deep, densely spaced tributary channels characterize the NE side and high fluvial terraces are absent. Older alluvial fan deposits have been truncated at their base, possibly initially by incision along the Waqia River; modern, low fluvial terraces in the main Waqia valley and tributary channels have been partially buried by a bajada extending ~5 km, which is juxtaposed against the older, truncated alluvial fan deposits (location 5, Fig. 2). In contrast, the SW side generally comprises comparatively undisturbed, glaciofluvial debris aprons incised by sparse tributary streams. Tall (>50 m), extensive fluvial terraces are present on the SW side of the main channel, and bajadas are absent in this location.

4.1. Paleolake Waqia shorelines and deposits

Shoreline notches and lacustrine deposits throughout the Waqia valley provide evidence for a large paleolake, that we call Paleolake Waqia (see Fig. 2, location 4 on the western valley bedrock and Fig. 3A). Three distinct levels of shoreline notches are visible in areas of high, exposed bedrock, most notably immediately W of the bedrock notch at elevations roughly ~3330–3230 m asl, ~17–70 m above the valley floor. These shoreline notches are also visible above the Waqia River where it flows into the Tashkurgan River.

Meters to tens-of-meters thick lacustrine deposits are present in most of the upper Waqia valley but are less common in the lower Waqia valley. The lacustrine deposits on the northeastern valley side are generally composed of thick (>20 m) beds of laminated silt overlain by fanglomerates. Cross-bedding and symmetric and asymmetric ripples are common in fine sands and silts within lacustrine deposits (Fig. 3B). Additionally, fine lacustrine sediments are exposed at higher elevations (e.g., between locations 8 and 9 in Fig. 2).

Soft-sediment deformation is common in fine-grained lacustrine deposits in the upper Waqia valley; load casts and flame structures are present at millimeter- to centimeter-scales, particularly in the upper Waqia valley deposits near the bedrock notch, load structures are visible in the upper and lower Waqia valley (e.g., at locations 1 and 8 in Figs. 2 and 3C), folding is common in upper Waqia valley deposits (Fig. 3D), and large-scale (tens of meters) tilted beds and clastic dikes are present in mid-upper Waqia valley deposits (Fig. 3E). The strike and dip of lacustrine beds varies significantly within the upper Waqia valley, e.g., at location 8 (Fig. 2), dip on both sides of the main valley channel generally ranges between 15° and 30° toward the N-NW, whereas at location 9 dip ranges between 25° and 35° to the north and across the main channel at location 10, <1 km away, and beds dip consistently to the ENE at 25°. Dropstones and ice-rafted debris are also present in many of these lacustrine deposits, in the upper and lower Waqia valley. The dropstones are typically small (<5 cm long axis) and are subangular to subrounded and deform the underlying strata (Fig. 3F).

The glacial deposits and landforms, fluvial terraces, erosional patterns, distribution of drainages, and shoreline elevations also define the boundaries of Paleolake Waqia in the upper Waqia valley. We interpret the hummocky deposits located SW of location 7 (Fig. 2) to be glacial and glaciolacustrine M-1 and M-2 stage ground moraines and ice-contact underwater fans or deltas. For the deposits from the western mountain range, concentrations of large boulders on hummocks and within fluvial channels are visible on satellite imagery from the proposed lake boundaries toward the mountain front, while such boulders are absent within the proposed lakebed. The character of these deposits varies distinctly from the mountain front to the proposed lakebed from well defined to subtle hummocks to smooth outwash plains. The T-3 fluvial terraces (see location 10, Fig. 2) define the location of a major drainage for the uppermost Waqia valley and suggest the former presence of significant volumes of water in the uppermost valley reaches.

4.2. Central-eastern Waqia sections

Fluvial incision along the upper Waqia valley has exposed sections tens of meters high through the valley fill sediments and landforms stretching many kilometers (locations 4–9 on the valley's NE side in Fig. 2; Figs. 4 and 5). Diamict deposits are complex, ranging from stratified to massive and matrix-supported and are many meters to tens of meters thick. Many diamict deposits are interbedded with stratified sands and gravels and, in places, planar-bedded silts. Deformation structures in the diamicts are complex and range from gently to steeply bedded regions to clastic dikes ~10 m high. These large deformation structures are more apparent when interbedded lacustrine silts and sands have been deformed concurrent with the over- or underlying diamicts (Figs. 3D, E, 5B and C).

The genesis of these deposits is not consistently obvious. In some locations, the diamict is clearly glacial as evidenced by the presence of bullet-shaped clasts (Fig. 6D), and cobbles and boulders are often rounded and of east and west Waqia valley provenance (Fig. 6C). At other locations the diamict contains shattered clasts, is locally clast-supported, and is more characteristic of landslide deposits as described by Benn and Owen (2002) and Hewitt (1999; Fig. 6A and B). These shattered diamict landslide deposits are common at the mouths of modern-day tributary valleys (e.g., Fig. 2, locations 1, 6, and 9) and along those valley sections, and can be traced across the valley from the central-eastern Waqia sections to exposures along the western side of the Waqia River.

4.3. Moraine M-1

Moraine M-1 is the highest and oldest moraine surface and is located ~300 m above the valley floor (Figs. 7A, 8A and B). Where sampled, the surface of M-1 is characterized by scattered, heavily weathered and heavily varnished but intact chert boulders ranging in size from a few centimeters to several meters in diameter (Table 1). Sparse chert cobbles with dark rock varnish are also present. The surface itself is largely covered in a <5-cm-thick unevenly distributed layer of loess. The loess is significantly eroded and presents as a sporadic 'cap' above the underlying diamict. All boulders are deeply inset in the underlying sediment.

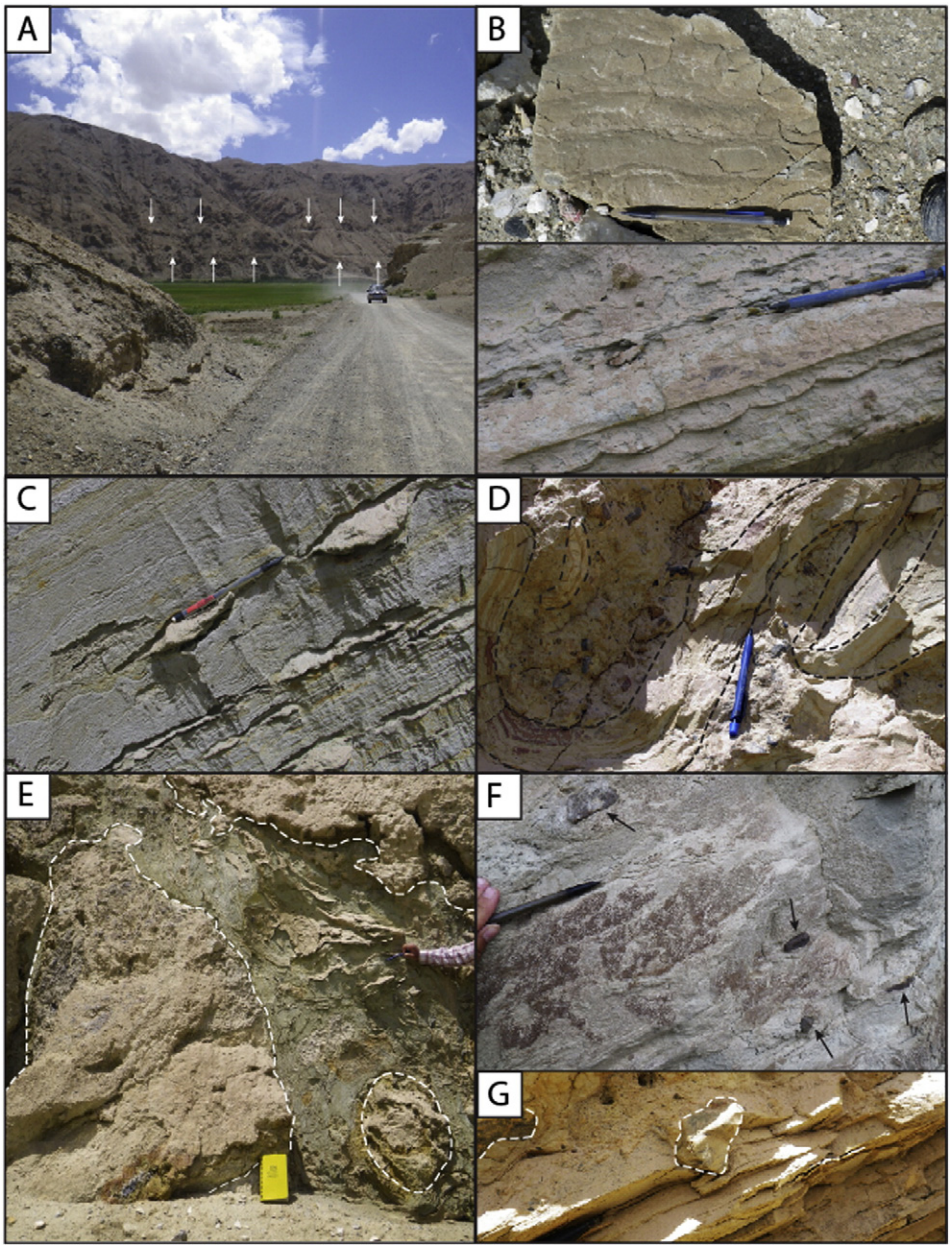

Fig. 3. Lacustrine landforms and deposits. (A) Shoreline notches cut into bedrock west of the bedrock notch (Fig. 2). View from location 4 on Fig. 2 looking west. Jeep for scale. (B) Asymmetric (top) and symmetric (bottom) in fine-grained sands. (C) Fine-grained sand load structures in finely laminated, folded silts and clay. (D) Overturned fold in silt (outlined in black), diamict between folds contains rip-up clast of silt layer. (E) Soft-sediment deformation of clays in the lower Waqia valley (location 3 on Fig. 2). Field notebook for scale. (F) Dropstones (black arrows) deposited in clay interbedded with fine sand with pen for scale (top; location 10, Fig. 2). (G) Succession of finely laminated silts overlain by ice-rafted debris, primarily coarse sand and gravel, including dropstones (dashed white line). Lacustrine silts above the ice rafted debris are deformed in folds at location 2 (Fig. 2). Pen tip for scale (lower left).

Additional remnants of the M-1 surface are visible to the NW of the sampling site (Fig. 2) but are generally constrained to thin caps of sediment and scattered boulders on ridges. Many intact, rounded to subrounded boulders on the valley floors may be eroded from M-1 deposits as discussed above.

Boulders on the M-1 moraine are primarily chert. Chert in the Waqia valley is sourced in the footwall of the Waqia Fault in the valley's eastern range; whereas the M-1 glacier advanced from the valley's western range. As such, interpretation of M-1 deposits must be carefully considered. The evidence is abundant for landsliding on the valley's eastern

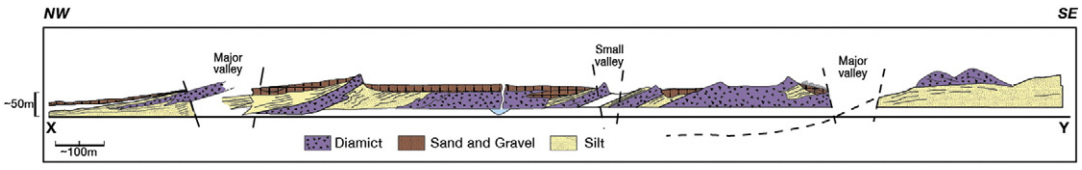

Fig. 4. Schematic field sketch of continuous exposures of the lacustrine, fluvial, and diamict deposits of the middle-eastern Waqia section showing lacustrine and gravel monocline and angular unconformity, general location of major valleys, and distribution of sediment types. See Fig. 2 for location of section.

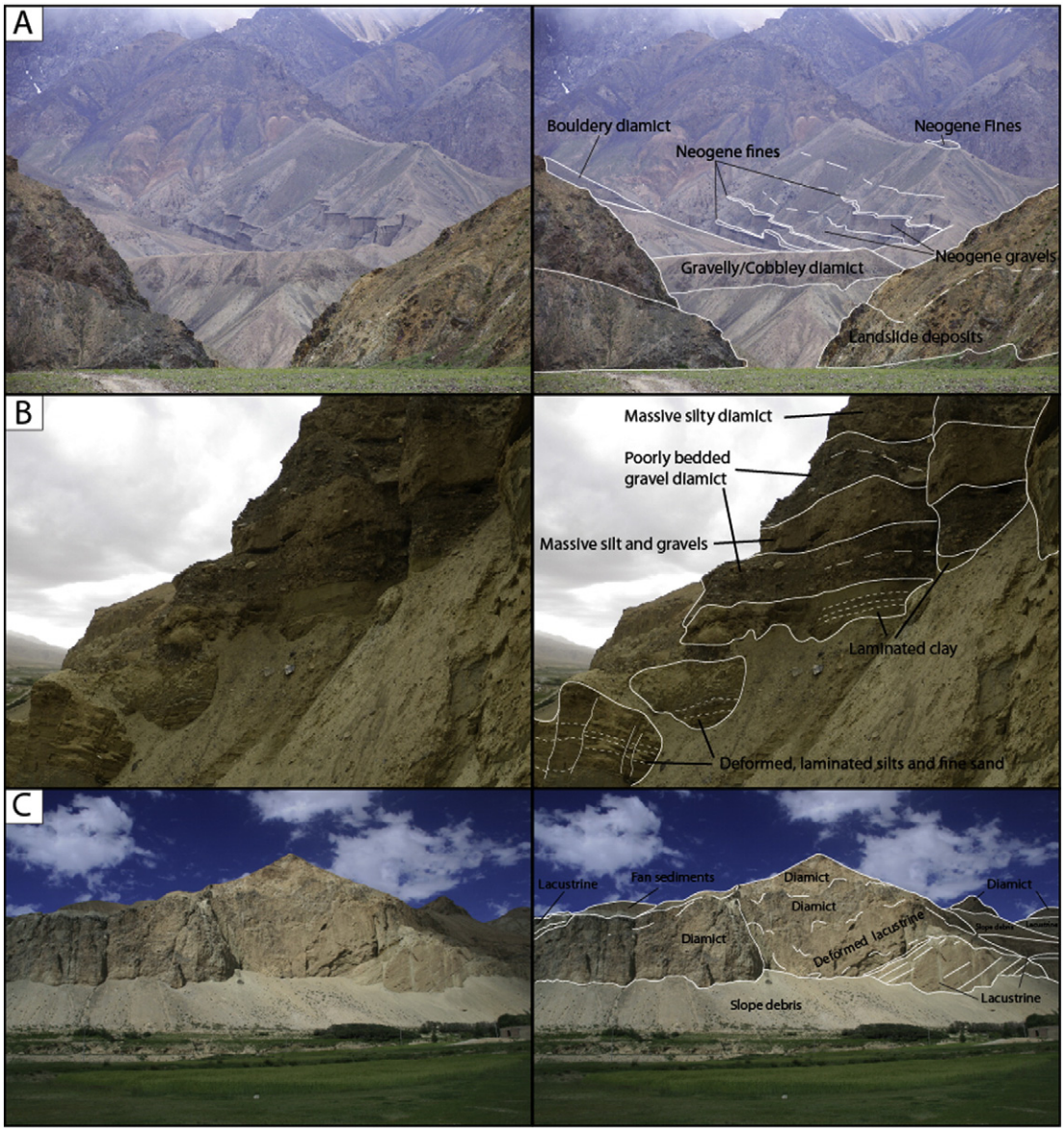

Fig. 5. Views of landforms and stratigraphic sections in the upper Waqia valley with (right) and without interpretation (left). (A) Alternating silts, sands, and coarse gravel deposits at higher elevations of location 9 (Fig. 2) tributary; photograph taken looking east-northeast. Cobbley/gravelly diamict and boulder diamict are likely Quaternary in age, possibly correlating to T-2 stage. (B) Stratigraphic section <100 m south from location 8 (Fig. 2). Section displays the complex sequence of lacustrine and fluvial/glaciofluvial erosion, deformation, and deposition and is proposed to be related to M-1 stage glacial advance. (C) Thick deformed lacustrine silts overlain and overlying diamicts at location 8 (Fig. 2). Upper diamict deposits in foreground are interpreted as glacial in origin (M-1); however diamicts in the far background may be remnant Neogene alluvial fan deposits.

side, which may be the initial source of chert boulders on the M-1 surface. However, the evidence indicating an extensive glacial advance into the former lakebed (dropstones and ice-rafted debris, sediment deformation, glaciolacustrine deposits) and the presence of a well-defined and extensive M-1 ground moraine ~2 km across the present-day valley at similar elevation (~50 m lower) suggests that the deposit has a glacial component as well. Significant glaciolacustrine, glaciofluvial, and debris flow deposits are associated with the M-1 advance, many of which are seen in deposits between locations 8 and 9 (Fig. 2) in close proximity to the M-1 deposits (~1.3 km); glaciofluvial and debris flow deposits are generally constrained to the boundaries of the proposed M-1 extent.

Large (>1 m), rounded granitic boulders are present in the valley floor immediately below the modern M-1 remnants, which suggests glacial transport from the valley's western side (hanging wall). We suggest that chert boulders in M-1 deposits originated from the footwall of the Waqia normal fault bounding the Waqia valley's eastern side and were later reworked into glacial deposits containing granitic boulders during M-1 glacial advance. Landsliding may also have deposited chert boulders on top of the M-1 glacial ice. Based on the factors discussed above, we interpret the M-1 sampling site to be glacial in origin.

4.4. Moraine M-2

The M-2 surface is relatively flat and is characterized by vegetation cover and minimal fluvial alteration restricted to larger, confined channels (Figs. 7B, 8C and D). Loess covers much of the surface in which a soil has developed. As a result of loess cover and selective denudation thereof, the majority of the clasts visible on the surface are large (>100 cm long axis) rounded boulders, although smaller boulders and cobbles are common in the beds of small drainage channels. We sampled large, inset, quartz-rich granitic boulders away from drainage channels (XJ98-100; Table 1). The sampled boulders were all located at a relative high point above secondary drainage channels and appeared 'fresh' with minimal or no rock varnish and were very hard and resistant to sampling. Lichen was present on all boulders.

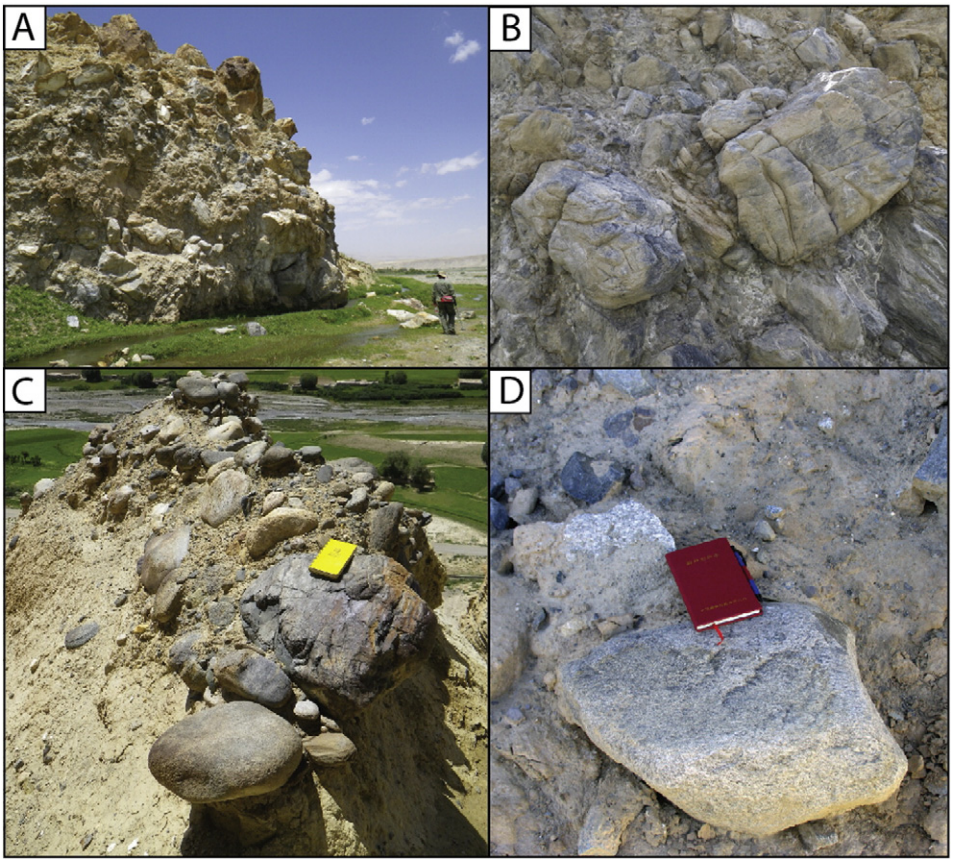

Fig. 6. Diamicts within the middle-eastern Waqia section. (A) View of massive matrix-supported landslide deposit at location 7 (Fig. 2). (B) Brecciated clasts forming jigsaw-like pieces (field of view ~50 cm) in landslide deposit in (A). (C) Glacial or glaciofluvial diamict with rounded cobbles and boulders of eastern and western mountain range provenance at location 8 (Fig. 2). (D) Bullet-shaped granite clast on M-2 surface.

4.5. Moraine M-3

Drainage channels dissect large areas of the western M-3 surface (Figs. 7D, 8E and F). However, the eastern portion grades from hummocky forms in the south to generally smooth outwash features to the north. Hummocks are broad with gentle slopes and generally are <5 m in height. All samples were collected in the southeastern portion of the M-3 surface. The surface is covered with thin but fairly regular vegetation and the soil is formed primarily from loess. The thickness of the loess is greatest at lower elevations and thins along hummock crests; there are few exposed boulders and sparse exposed cobbles in the lower regions of the M-3 surface, with exposed clasts concentrated primarily on the top or sides of hummocks. Boulders sampled on the M-3 surface include granite, granodiorite, diorite, and granite with a slight foliation (metagranite). Sampled boulders were located at the top of hummocks and were well inset in the underlying sediment. Many of the boulders had surfaces that appeared 'fresh' and lacked rock varnish except on the boulder sides, where varnish typically was well developed. Orange lichen was most typically only located on the side of boulders. The lack of rock varnish or lichen growth might suggest exfoliation or erosion of the boulder surface, but despite this, all boulders were hard and resistant to sampling.

4.6. Moraine M-4

Fluvial erosion has isolated the M-4 surface at ~20 m above the valley floor (Figs. 7E, 8G and H). The M-4 surface is characterized by broad, smooth hummocks and sparse elongate ridges topped with vegetation ranging from thin and patchy to a regular cover. Exposed boulders are concentrated primarily on ridge crests, while lower-lying areas are covered in a thin layer of pedogenized loess with sparse exposed cobbles and very few boulders. Boulders on the M-4 surface are primarily composed of foliated granite and are >100 cm long.

4.7. Moraine M-5

Moraine M-5 is a hummocky moraine with similar vegetation cover to that of M-3 and M-4. However, M-5 hummocks are smaller and higher in relief than those of the other surfaces (Figs. 7F, 8I and J). Although exposed clasts are more regularly found on the tops of hummocks, the concentration of boulders and cobbles on these areas is much greater than on the M-3 and M-4 surfaces. Cobbles dominate the exposed clasts. Boulders on the M-5 surface are smaller and more low-lying, though they are still deeply inset and display patchy, dark rock varnish and orange and black lichen. The degree of rock varnish was variable even on the same boulder.

4.8. Moraine M-6

The M-6 moraine is a hummocky moraine with less distinct ridges than most of the other surfaces located far upvalley of all the other moraines, ~2 km from the modern glaciers (Figs. 7G, 8K and L). High relief mountainsides bound the surface, and mass wasting of material from the surrounding slopes is possible. Care was taken to sample boulders well inset into the surface and as far from valley walls as possible. The M-6 moraine is modified by periglacial processes, resulting in areas of patterned ground (frost-crack polygons and stone garlands) and evidence of frost heave; the surface is littered with abundant, angular boulders, which in some locations are concentrated in a small, elongated area. Vegetation on the surface is relatively thick but somewhat uneven where periglacial processes have disrupted the soil. Boulders sampled

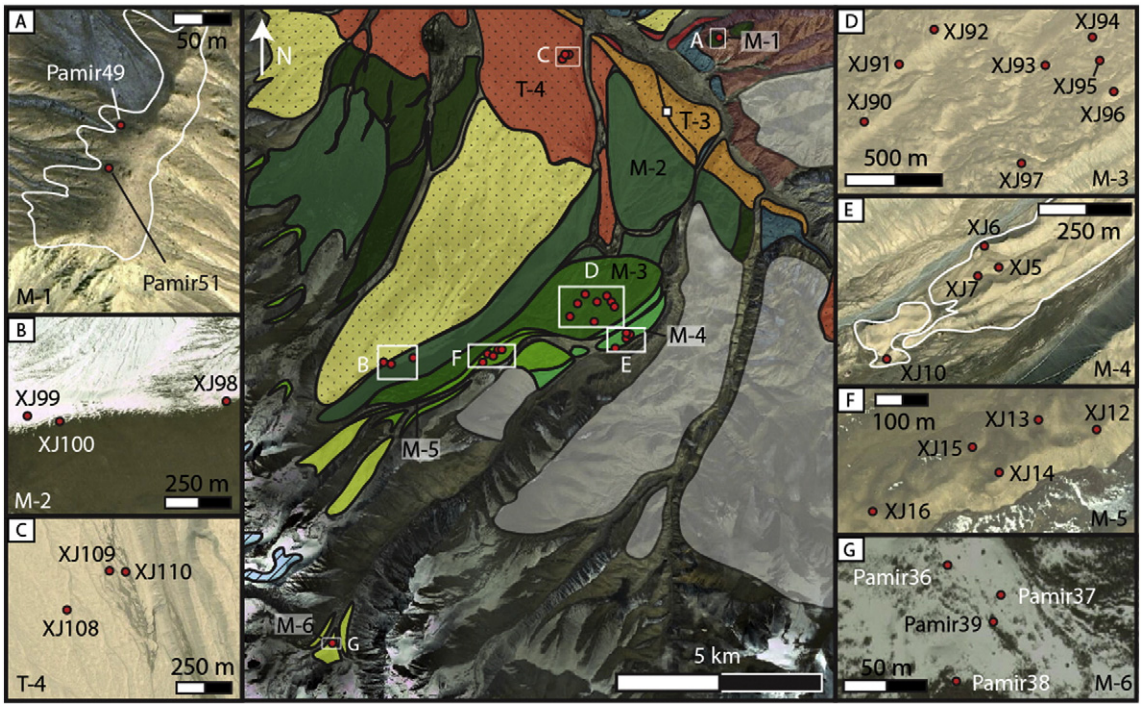

Fig. 7. Detailed images showing moraines and sample locations for ^{10}Be dating (red dots). White lines, where present, outline the extent of moraine deposits as labeled. Images from Google Earth. The location of depth profile on T-3 is shown by the small white square.

on this surface were low-lying, angular quartzites slightly inset into the surface. Despite the proximity to the modern glacier and source area, which suggests a young landform age, these boulders displayed a well-developed rock varnish, darker than that on boulders or any other sampled surface, suggesting an older exposure age. The M-6 boulders are also covered in abundant orange and white lichen.

4.9. Alluvial fan surface T-1

The T-1 is an alluvial fan surface located north of the bedrock notch that separates the upper and lower Waqia valley (Fig. 2). In this area of the lower Waqia valley, the Waqia River is confined to a narrow channel to the west with exposed bedrock reaching >500 m above the valley floor and to the east by extensive alluvial fan deposits >10 m thick and older Neogene deposits. The T-1 surface is primarily composed of schist and marble transported from the northeastern range front. Loess deposits are present across the majority of the surface and, where investigated, vary in thickness from <10 to ~30 cm. A thin crust is present on much of the higher-elevation loess surfaces. No boulders or cobbles are visible on the alluvial fan surface because of the loess cover, although small (<3-cm-long axis), angular (schist) to subrounded (quartz) pebbles are common. Numerous, small fluvial channels have contributed to mild bar and swale features typically varying in height by <50 cm. This character changes closer to the range front where more extensive fluvial incision has eroded away much of the T-1 surface to the east resulting in the removal of the loess cover and in the deposition of darker sediment, primarily clasts composed of low-grade schist. This represents a younger phase of alluvial fan development present dominantly on the alluvial fan surface near the range front and in the modern distal drainage channels.

The sampled area of T-1 is a broad, loess-covered plain ~5 km from the range front characterized by gentle bars and swales, probably formed by a combination of fluvial and aeolian action. Larger drainage channels are present >5 m from the sample site. The XJ102 depth profile pit was dug into the crest of a ~3 m-wide bar. A poorly developed red surface soil is present to ~5–10 cm depth; and red paleosols, clay, and intense clast grussification are common within the upper 70 cm of the section. The entire section is rich with fine silt deposits and angular schist clasts, primarily in pebble-sized clasts but also in boulders. Rounded, non-schistose clasts are rare, but when present they are typically composed of marble and are pebble-sized.

4.10. Alluvial fan surface T-2

The T-2 deposits are extensive laterally and perpendicular to the range front, spanning a distance of ~3.5 km from the range front to the present river channel. These deposits probably belonged to a large bajada system, now deeply incised by streams originating from the range to the east. The alluvial fan deposits are ~200 m thick at their toe where exposed along the Waqia River.

The T-2 is covered in a variable <30-cm-thick layer of loess with small bars and swales probably influenced primarily by aeolian processes and secondary fluvial drainages, typically incised <1 m. Boulders and cobbles are absent on the alluvial fan surface, but small, subangular pebbles are common. The XJ104 depth profile pit is located ~2.5 km from the range front on a gently undulating, loess-covered portion of the surface, >30 m from any larger drainage channels. Similar to the T-1 pit, the section showed limited soil development within the first ~5 cm and red paleosols and grussification common to ~30 cm depth. Particle sizes were bimodal with significant amounts of silt and pebbles, and sparse boulders.

4.11. Terrace T-3

Terrace T-3 is a ~1-km-wide terrace located ~100 m above the main valley floor at the base of the M-3 moraines. T-3 deposits have been incised into and reworked at their NE extent by the Waqia River and its tributaries, resulting in a younger and lower terrace flanking the deposit (Fig. 2). The position and morphology of the T-3 terrace suggests that it may be a fluvially reworked remnant of the M-3 moraine deposits with later fluvial modification in the form of deeply-incised (>20 m) channels in the T-3 surface. Loess cover varies between ~5 and ~40 cm. Clasts

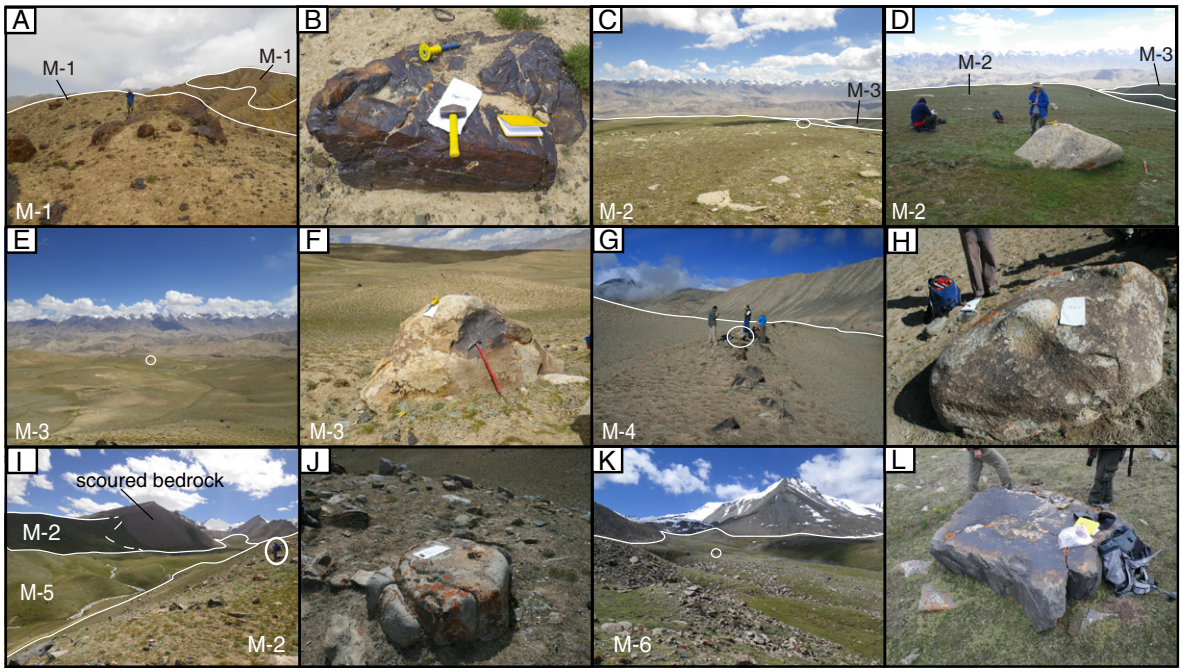

Fig. 8. Views of moraines (left column) and examples of sampled boulders (right column) for each glacial stage (M-1 though M-6). Where present, white lines outline the boundaries between different surfaces. (A) M-1: View from Pamir-51 sample location looking northeast at continuation of the M-1 moraine (note person for scale). (B) M-1: Pamir-51 sampled boulder. (C) M-2: View looking east across Waqia Valley with M-3 in the background from between samples XJ98 and XJ100. People (circled) for scale. (D) M-2: XJ98 sampled boulder. (E) M-3: View to the east across the M-3 surface. The circled boulder is sample boulder XJ90. (F) M-3: Sampled boulder XJ90. (G) M-4: View from the M-4 ridge to the southwest. (H) M-4: Sampled boulder XJ7. (I) M-5: View from M-2 surface looking down onto M-5. (J) M-5: Sampled boulder XJ13. (K) M-6: View to the south from the valley approach (note person in the circle for scale). (L) M-6: Pamir36 sampled boulder.

of any size are rare on the T-3 surface, and because thicker and more stable loess cover, the surface is covered in sparse vegetation and many areas have developed a thin soil. Deeply-incised drainages have exposed deposits under the loess that are rich in well-rounded boulders, typically ~30 cm in diameter. The XJ103 depth profile pit was dug into the side of a large drainage where loess cover was <5 cm. The depth profile sediments comprised clast-supported deposits dominated by well-rounded boulders (25–40 cm) and cobbles with some pebbles. No paleosols were observed, but roots and clay were apparent in the top ~5 cm of sediment and clasts within top ~35 cm were grussified.

4.12. Alluvial/glaciofluvial wash fan surface T-4

The surface of T-4 is incised by numerous small channels (Fig. 7C) and populated by sparse boulders reaching 50 cm in diameter and of variable lithology including granite and vein quartz with cobbles and pebbles similarly sparse. The surface exhibits significant but variable loess cover, typically ~5–20 cm thick, which has undergone fluvial erosion, creating a channeled surface with a bar and swale-like topography. Boulders were sampled on the crests of bars where they have higher relief and loess cover is thinner.

5. Ages of moraines and alluvial fans

All ^{10}Be data, ages, surface variables, and boulder characteristics are presented in Tables 1 to 3 and our assigned ages to landforms are summarized in Tables 3 and 4. Individual boulder ages range from 2 to 124 ka (Fig. 9). Depth profile data results are shown in Table 2 and Fig. 10. All the exposure ages should be considered as minimum ages for the landforms we dated, and the associated uncertainties were discussed above.

Depth profile simulations show that the T-1 alluvial fan surface is the oldest dated landform in the Waqia valley with an age that is constrained to be between ~463 and 904 ka, with a best estimate of ~582 ka (Table 2). This age is significantly older than all other dated landforms in the Waqia valley.

Monte Carlo simulation for T-2 (depth profile XJ104) suggests an age between ~103 and 208 ka, with a best estimate of ~120 ka. The T-2 probably formed through fluvial processes before or during the M-1 glacial advance as the glacially confined lake in the uppermost Waqia valley was partially or completely drained, possibly over a period of several hundred to thousands of years. The T-2 tops thick lacustrine deposits associated with the lacustrine deposits upvalley deformed by loading because of the advance of the M-1 glacier.

Although we originally sampled four boulders on M-1, only two provided sufficient quartz for dissolution and ^{10}Be extraction. Samples from M-1 boulders yielded ages of 78.5 ± 10.0 ka (Pamir-51) and 33.3 ± 3.0 ka (Pamir-48). The M-2 surface boulders yielded ages of 40–75 ka (XJ98, 74.8 ± 7.2 ka; XJ99, 60.2 ± 5.3 ka; and XJ100 40.1 ± 3.6 ka). Overlap in the older boulder exposure ages between M-1 and M-2 may be explained by a variety of possibilities, including: (i) deposition of boulders occurred either roughly contemporaneously (M-1 and M-2 are approximately the same age); (ii) glacial advance during the M-2 stage incorporated and reworked boulders from earlier M-1 deposits (M-1 is an unknown age older than M-2); and (iii) older M-1 boulder ages are not representative of surface age because boulders having been buried or experiencing extreme erosion (M-1 is an unknown age older than M-2). Overlap in and distribution of younger boulder exposure ages in M-1 and M-2 deposits may be explained by disparate burial and therefore exposure histories in that boulders that have been buried for a significant amount of time or whose surface has experienced erosion may result in a much younger age than is representative (for more explanation and a detailed description behind the rationale for this interpretation see Dortch et al., 2013).

The M-1 and the M-2 surfaces differ significantly in boulder lithology, surface and boulder characteristics, and modern landform morphology. Boulders present on the M-1 surface are primarily composed of chert, whereas boulders on the M-2 surface are consistently metamorphosed granites. Boulders present on the M-1 surface exhibit more

developed rock varnish than those of M-2 and are generally significantly smaller than those on the M-2 surface (Fig. 4B and D). Differing rock varnish may be primarily due to lithologic differences, although it may also indicate a significantly longer exposure of the M-1 boulders. This may also be true of the differing boulder sizes between the M-1 and M-2 deposits; weathering of the M-1 boulders may be lithologically influenced or weathering and denudation of the M-1 surface may have been far more extensive than that of M-2, resulting from and indicative of a long history of burial for M-1 boulders. The morphology of the M-1 surface is characterized by disconnected remnant deposits in some areas separated by deeply-incised fluvial channels and significant elevation (Fig. 2) that differs greatly from that of M-2 and suggests extensive denudation of M-1 deposits. Significantly better preservation of the M-2 landform surface and boulders probably indicate a significant age difference in the M-1 and M-2 deposits, and a much older age for the M-1 moraine.

Because of the small sample size and significant range in reported ages and the above reasoning, we suggest an age much older than 80 ka for M-1, possibly concurrent with the age of formation of T-2 between 103 and 208 ka. This is because glacial advance correlates with a drop in paleolake level and formation of the T-2 in areas vacated by lake water. This would also be coincident with the penultimate glacial (MIS 6) or earlier. We tentatively correlate M-1 with the Dabudaer glacial stage of Owen et al. (2012) for the Tashkurgan valley, but acknowledge the possibility that landslides to the east may have contributed boulders to the M-1 as discussed above (Section 4.3).

The M-2 might have been formed at ~80 ka based on the age of its oldest dated boulder. However, M-2 may be significantly older than 80 ka. This is because ~80 ka was an interstadial time (MIS 5a), and the climatic conditions were unlikely favorable enough for the development of extensive glaciers, nor throughout the interstadials-interglacial times of MIS 5a-e (interstadial-interglacial times defined by Martinson et al., 1987). We therefore favor a penultimate glacial age for this advance. Furthermore, T-2 with an age range of 103 to 208 ka is associated with M-1, and M-2 is possibly younger than this terrace is coincident with the later part of this age range during late MIS 6. The M-2 is likely coincident with the Dabudaer glacial stage of Owen et al. (2012). Owen et al. (2012) argued that the Dabudaer glacial stage in the Tashkurgan valley probably represents several significant glacial advances, and it is therefore reasonable to correlate M-1 and M-2 to the Dabudaer glacial stage.

The T-3 and T-4 terraces were formed after deposition of M-2 glacial sediments because the T-3 terrace was cut directly into M-2 glacial deposits and because the T-4 fluvial outwash surface is juxtaposed against the M-2 lateral moraine. The T-3 and T-4 surfaces are similar in elevation (~3475 m asl at each sample site) but probably experienced different depositional and erosional histories: T-3 formed primarily through glacial deposition followed by fluvial erosion, and T-4 formed primarily as deposition as a glacial outwash feature. Depth profile and ^{10}Be dating suggest an age of ~100 ka for the T-3 surface and ~70 ka for the T-4 surface (see Table 4).

The spread of ages for M-3 is large but shows two clusters: one at ~55 ka (XJ90 at 59.3 ± 5.5 ka, XJ94 at 50.7 ± 6.0 ka, XJ95 at 53.2 ± 4.8 ka, and XJ97 at 51.2 ± 4.8 ka), and another at ~15 ka (XJ91 at 16.9 ± 1.6 ka and XJ92 at 13.5 ± 1.2 ka). Samples XJ93 (37.3 ± 3.2 ka) and XJ96 (20.8 ± 1.6 ka) have ages that are beyond 2σ outliers of the average age. We favor the older ages in the cluster because the younger ages might represent weathered boulders and assign M-3 to early last glacial (MIS 4) and correlate it with the Tashkurgan glacial stage of Owen et al. (2012) in the Tashkurgan valley and with the SWHTS4 stage of Dortch et al. (2013) in the semiarid western regions of the Himalayan-Tibetan orogen.

The M-4 boulders give ages of 15 to 30 ka (XJ5, 14.9 ± 1.4; XJ6, 30.3 ± 2.7 ka; XJ7, 15.0 ± 1.5 ka; XJ10, 21.4 ± 2.2 ka). The moraine represents a last glacial advance, possibly late MIS 2. The M-4 is probably correlated with the Kuzigun glacial stage in the Tashkurgan Valley of Owen et al. (2012) and the SWHTS2D/E stage of Dortch et al. (2013) for the semi-arid regions at the western end of the Himalayan-Tibetan orogen.

Boulder ages from the M-5 moraine range from 8 to 15 ka (XJ12, 10.8 ± 1.0 ka; XJ13, 8.0 ± 3.6 ka; XJ14, 14.8 ± 1.4 ka; XJ15, 14.8 ± 1.3 ka; XJ16 8.2 ± 0.7 ka). The M-5 probably represents a Late Glacial advance and likely correlates with stage SWHTS2A to 2C of Dortch et al. (2013) for the semi-arid regions at the western end of the Himalayan-Tibetan orogen.

Boulder ages for the M-6 moraine range from 2 to 11 ka (XJ36, 7.6 ± 0.9 ka; XJ37, 1.5 ± 0.2 ka; XJ38, 11.6 ± 1.2 ka; XJ39, 10.4 ± 2.5 ka) and probably represent an early Holocene glacial advance correlated with the SWHTS1E stage of Dortch et al. (2013) for the semi-arid regions at the western end of the Himalayan-Tibetan orogen.

6. Quaternary landscape development

The development and history of the Waqia valley, as summarized in Fig. 11, provide a model for the landscape evolution of Himalayan-Tibetan valley systems to help in examining the interplay among tectonics, climate, deposition, and erosion. The study shows that the valley has experienced a succession of punctuated depositional and erosion events on a 10^4-year timescale.

Table 4
Summary of all ages from depth profile and surface boulder ^{10}Be dating.

Surface name	Surface sample type	Maximum age (ka)	Minimum age (ka)	Mean age and 2σ uncertainty (ka)	Probability density function age (ka)[a]	MSWD age (ka)	Most likely age[b]	Correlation of moraines with Tashkurgan Valley	Correlation with SWHTS of Dortch et al. (2013)
M-1	Surface clasts	78.5 ± 10.0	33.3 ± 3.0	–	73.4	–	Penultimate glacial cycle or older	Dabudaer glacial stage	SWHTS6 or older
M-2	Surface clasts	74.8 ± 7.2	40.1 ± 3.6	58.4 ± 17.4	**60.0** 25.0–25.2	–	Penultimate glacial cycle (MIS 6)	Dabudaer glacial stage	SWHTS6 or older
T-3	Depth profile	162	82	–	**97.1** 81.6–161.6	–	~100 ka	n/a	n/a
T-4	Surface clasts	124.1 ± 11.1	59.5 ± 5.4	63.2 ± 5.2	**68.0** 16.3–72.1	–	Early last glacial (MIS 4 or older)	n/a	n/a
M-3	Surface clasts	20.8 ± 2.0 59.3 ± 5.5	13.5 ± 1.2 37.3 ± 3.2	17.0 ± 3.7 50.3 ± 8.1	−59.7	−53.5 ± 4.0	Early Last Glacial (MIS 4)	Tashkurgan glacial stage	SWHTS4
M-4	Surface clasts	30.3 ± 2.7	14.9 ± 1.4	20.4 ± 7.3	**17.8** 0–16.0	–	MIS 2	Kuzigun glacial stage	SWHTS2E
M-5	Surface clasts	14.8 ± 1.3	8.0 ± 3.6	11.3 ± 3.3	**11.3** 5.6–7.4	–	Late Glacial	n/a	SWHTS2A-2C
M-6	Surface clasts	11.6 ± 1.2	1.5 ± 0.2	9.9 ± 2.1	10.4	–	Early Holocene	n/a	SWHTS1E

– indicates no data; n/a indicates not applicable.
[a] All probability density function age values based off of ^{10}Be cobble/boulder data. Values in bold are the best estimates.
[b] Most likely age is determined by dating results within the context of the geomorphic landscape.

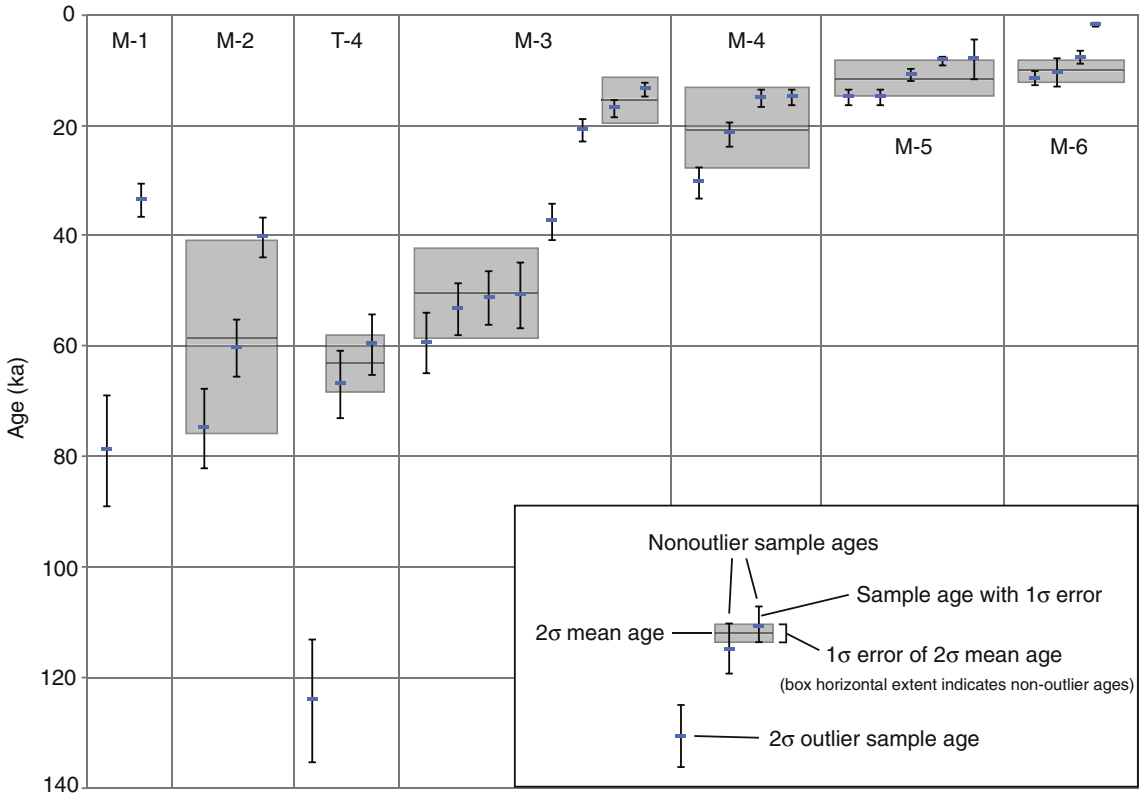

Fig. 9. ^{10}Be ages for sampled boulders. Ages are plotted by relative age of landform (M-1 to M-6; T-4), and within each landform sample ages are arranged from oldest to youngest boulder age. For each age the uncertainty is shown as 1σ, which includes analytical and production rate uncertainty.

The oldest sediments in the study area, excluding bedrock, include thick (>1000 m) Neogene alluvial fan, and fluvial, lacustrine, and landslide deposits. These occur along the modern-day Waqia valley as remnants (Fig. 11A). Many of these older deposits are enigmatic and represent multiple stages of deposition and erosion resulting in thick (>300 m) deposits composed of multiple unconformable units. A full description and interpretation of the Neogene sediments is beyond the scope of this study, but these deposits record a time of extensive valley sedimentation, with the deposits totally filling the valley in places. The Neogene deposits have been deformed into open folds and monoclines throughout the late Cenozoic as a response of the Indian-Asian collision and then subsequently eroded.

Diamicts, including metre-size boulders, sporadically cap the Neogene deposits in the upper Waqia valley (e.g., location 9, Fig. 2). These diamicts probably represent post-Neogene landslide deposits of broader lateral extent. A large lake, Paleolake Waqia, submerged much of the basin after the deposition of these landslide deposits, but before formation of the T-1 alluvial fan (Fig. 11B). At least three shoreline notches, visible in the lower and upper Waqia valley, show that Paleolake Waqia had at least three distinct high stands (Fig. 3A). The highest shoreline shows that the lake covered most of the upper Waqia Valley to the Yarkand River (Figs. 2 and 11A).

The nature of formation of Paleolake Waqia is unknown, but it may have been glacially dammed on numerous occasions; or it may have been the result of landslide dams. The formation of Paleolake Waqia resulted in deposition of thick, extensive clays, silts, and fine sands (Fig. 11B). Contacts between Neogene and Paleolake Waqia deposits are not clear in the field; many key areas are obscured because of mass wasting. Lacustrine sediments are best preserved on the northeastern side of the valley where they are glaciotectonised into a monocline (Fig. 2, between locations 5 and 9; Fig. 6) and display evidence of soft-sediment deformation, most notably at location 8 (Fig. 2); this deformation is further discussed below. Deposits of sand that coarsen toward the mountain front characterize the margins of Paleolake Waqia (Fig. 11B). In some areas thin lenses of gravels with well-rounded clasts suggest continued fluvial input from channels exiting the northeastern mountain front, and the presence of dropstones and lenses of ice-rafted debris in silt and clay indicate the presence of glacial ice. Abundant coarser deposits including rounded fluvial or glaciofluvial boulders and cobbles have been deposited as sets of distinct beds, or disordered clusters are present near the center of the upper valley (Fig. 2, location 8; Fig. 6). These overlie many of the lacustrine units, which are best exposed along the truncated alluvial fans and deeply-incised tributary channels on the eastern side of the valley. The T-1 alluvial fan appears to be largely undisturbed, which suggests it was a long-lasting landform (Fig. 11B). The T-1 surface is ~100 m lower than the highest shoreline notch, and hence Paleolake Waqia must have been at its maximum extent earlier than 580 ka.

Fluvial deposition along the Waqia valley's northeastern mountain front resulted in thick and extensive alluvial fan deposits and the formation of T-2 probably during MIS 6 (Fig. 11B). Although the relative timing of landform development is not entirely clear, T-2 is probably older than the M-1 glacial deposits; the M-1 moraine deposits, although at a similar elevation to T-2, are juxtaposed against remnant alluvial fan surfaces above Neogene deposits near the M-1 moraine's greatest extent. High remnant alluvial fan surfaces up tributary valleys to the northeast of the most extensive M-1 deposits suggest much more expansive alluvial fan deposits existed before the M-1 glacial advance and before erosion of previous alluvial fan deposits. The T-2 alluvial fans formed either concurrently or before the M-1 advance and, if so, M-1 ice probably overran parts of the T-2 that was not preserved.

The M-1 stage glaciers advanced to the lakeshore possibly during a third and lower lake stand of Paleolake Waqia after the formation of T-1 and T-2 (Fig. 11B), as is evident from dropstones (Fig. 3F) and lenses

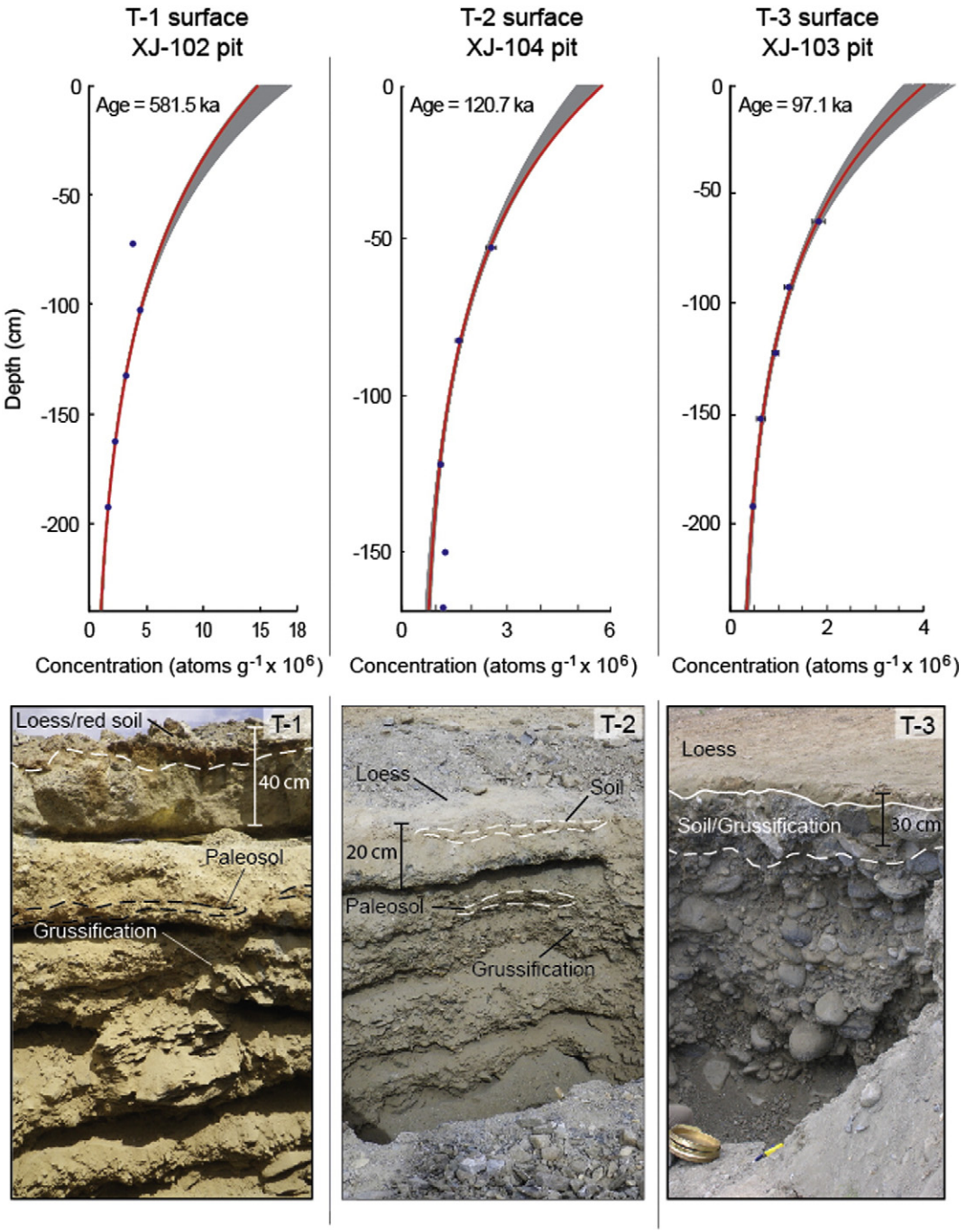

Fig. 10. Depth profile curves for T-1 (XJ-102), T-2 (XJ-104), and T-3 (XJ-103) for ^{10}Be concentrations. Grey lines represent a bulk analysis of 100,000 iterations and red curves show best-fit results using Hidy et al.'s (2010) Monte Carlo simulator as described in Section 3.2. The photographs show views of each depth profile pits arranged below the corresponding curves.

of ice-rafted debris at multiple locations in lacustrine deposits. Dropstones are present in the upper and lower valley (e.g., Fig. 2, location 1). The hummocky deposits on the western side of the upper Waqia valley are probably ice-contact fan deltas. Significant input of sediment from the mountain front along the Waqia valley's northeastern side may have resulted in lake shoreline migration toward the southwest mountain front (Fig. 11C). An extensive bajada, spanning the NE side of the upper Waqia valley, formed during this time (e.g., at locations 4 and 6 in Fig. 2).

In the lower Waqia Valley south and upvalley of T-1, dropstones and load structures are present at several locations (Fig. 2, locations 1 and 2). Distinctive sediment loading structures (Fig. 3), in addition to the presence of dropstones upvalley from the proposed Paleolake Waqia extent, imply the presence of glacial ice within the tributary valley. These deposits are enigmatic as they suggest the presence of a large glacier originating from the northeastern valley side (Fig. 11B), where evidence for glaciation is sparse compared to the upper valley. The location of this glacier was likely controlled by the presence of the large landslide scarp, which created a rare, north-facing catchment favorable to accumulating significant ice (Fig. 11B).

The continued advance of a glacier across the lake in the upper Waqia valley resulted in the formation of the large M-1 moraine. This glacier and associated landforms resulted in the formation of smaller lakes in many of the existing tributary valleys upvalley from M-1

moraines (Fig. 11B and C). Soft-sediment deformation in the Waqia lacustrine deposits (Fig. 6C) is probably primarily linked to M-1 glaciations in the upper Waqia valley. Many of the Waqia valley's lacustrine sediments near the preserved M-1 glacial deposits are tilted (Fig. 5) and exhibit soft-sediment deformation (Fig. 5C), above which are deposited thick glacial diamicts (Fig. 6C). In combination, these factors suggest that loading and deformation of the lake sediment because of the presence of an overriding glacier.

Drainage of the Paleolake Waqia and smaller upvalley lakes dammed by M-1 glacial debris may have occurred concurrently or in stages. The M-2 glacial advance resulted in the deposition of extensive deposits within the former M-1 glacier's extent and probably helped to dam drainage (Fig. 11C). The T-3 terraces were formed by incision of the proto-Waqia River through M-2 sediments (Fig. 11D), which requires at least partial lake drainage by ~100 ka. The T-4, located adjacent to M-2 glacial deposits, formed as runoff from the M-2 glacial advance and retreat expanded over the vacated lakebed of the former Paleolake Waqia. Drainage of the lake and the resulting establishment of the Waqia River and lowering of base level resulted in deep (>100 m) incision of tributary valleys through T-2 alluvial fan surfaces and underlying lacustrine and Neogene deposits (and bedrock in places). Over time erosion by the Waqia River caused

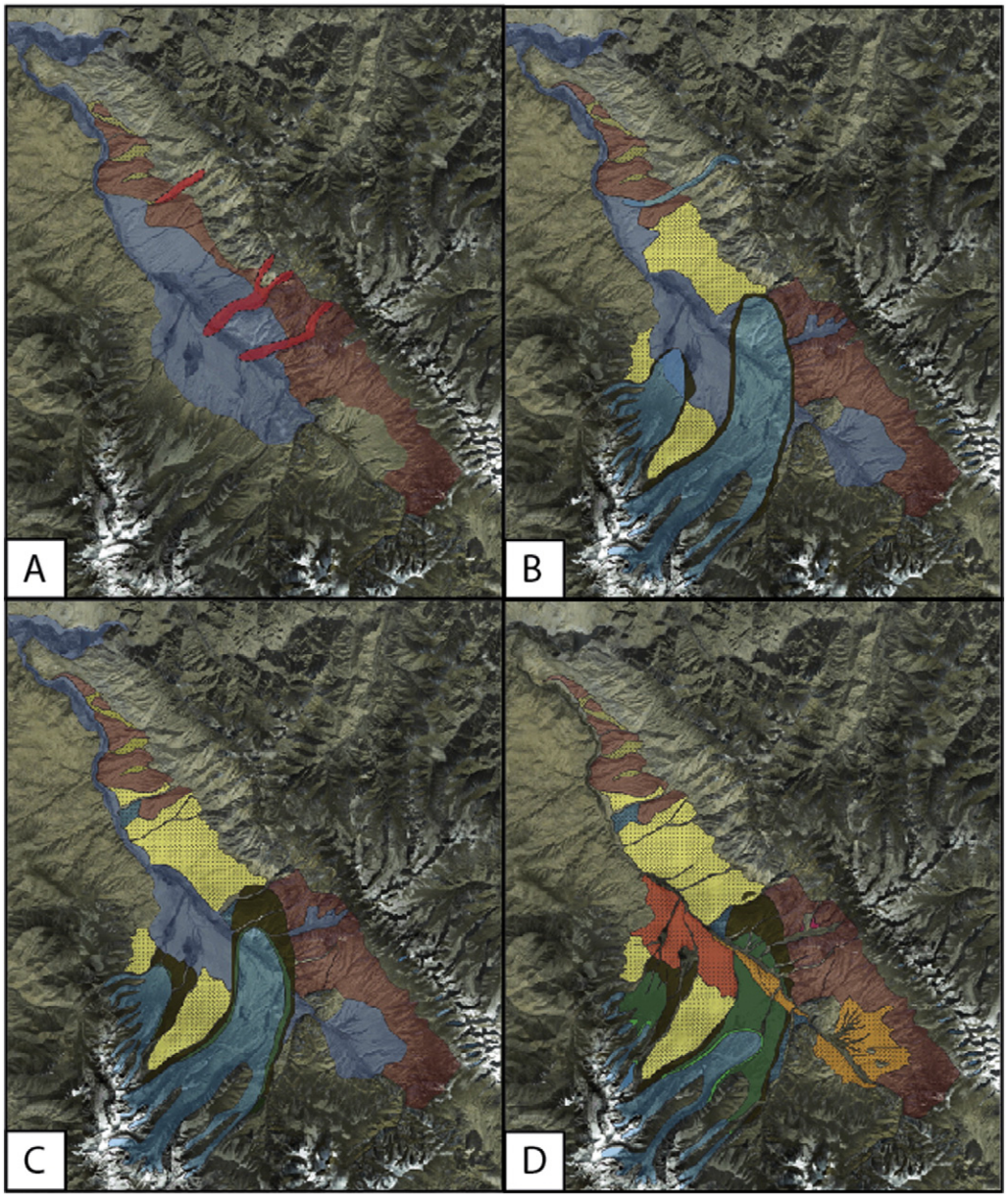

Fig. 11. Schematic figures showing the simplified Quaternary geomorphic evolution of the Waqia valley. (A) Formation of Paleolake Waqia above and against Neogene deposits. Landsliding occurred prior to or concurrent with lake formation. T-1 terraces were formed within this time period. (B) T-2 surface is deposited likely before but possibly concurrently with M-1 advance. M-1 glacial advance from the southwest side of the valley erodes Neogene and Quaternary alluvial fan sediments, deforms underlying lake sediments, and leaves extensive M-1 glacial deposits causing ice and debris damming of upvalley catchments. (C) M-2 advance deposits M-2 moraines resulting in continued damming of upvalley catchments. Erosion of moraines and retreat of ice after this allows for draining of all upvalley dammed lakes, results in the formation of T-3. Drainage of Paleolake Waqia proper allows for formation of T-4 outwash fans on Waqia's southwest side as a product of glacial outwash from the M-2 stage and additionally lowers tributary valley base level, allowing for tributary channel incision. (D) M-3 glacial advance and deposits. (E) M-4 glacial advance and glacial deposits. Continued erosion of deposits from previous glacial advances and further incision of the Waqia River truncating T-2 and underlying lacustrine deposits. (F) M-5 glacial advance and deposition. (G) M-6 glacial advance and deposit of M-6 moraine. Continued fluvial erosion of glacial deposits in tributaries. (H) Waqia River continues to incise into valley resulting in multiple small terraces along the modern river valley and deposition of small alluvial fans at the mouths of tributary valleys. Mass deposition of loess on surfaces in the valley's southeast extremes.

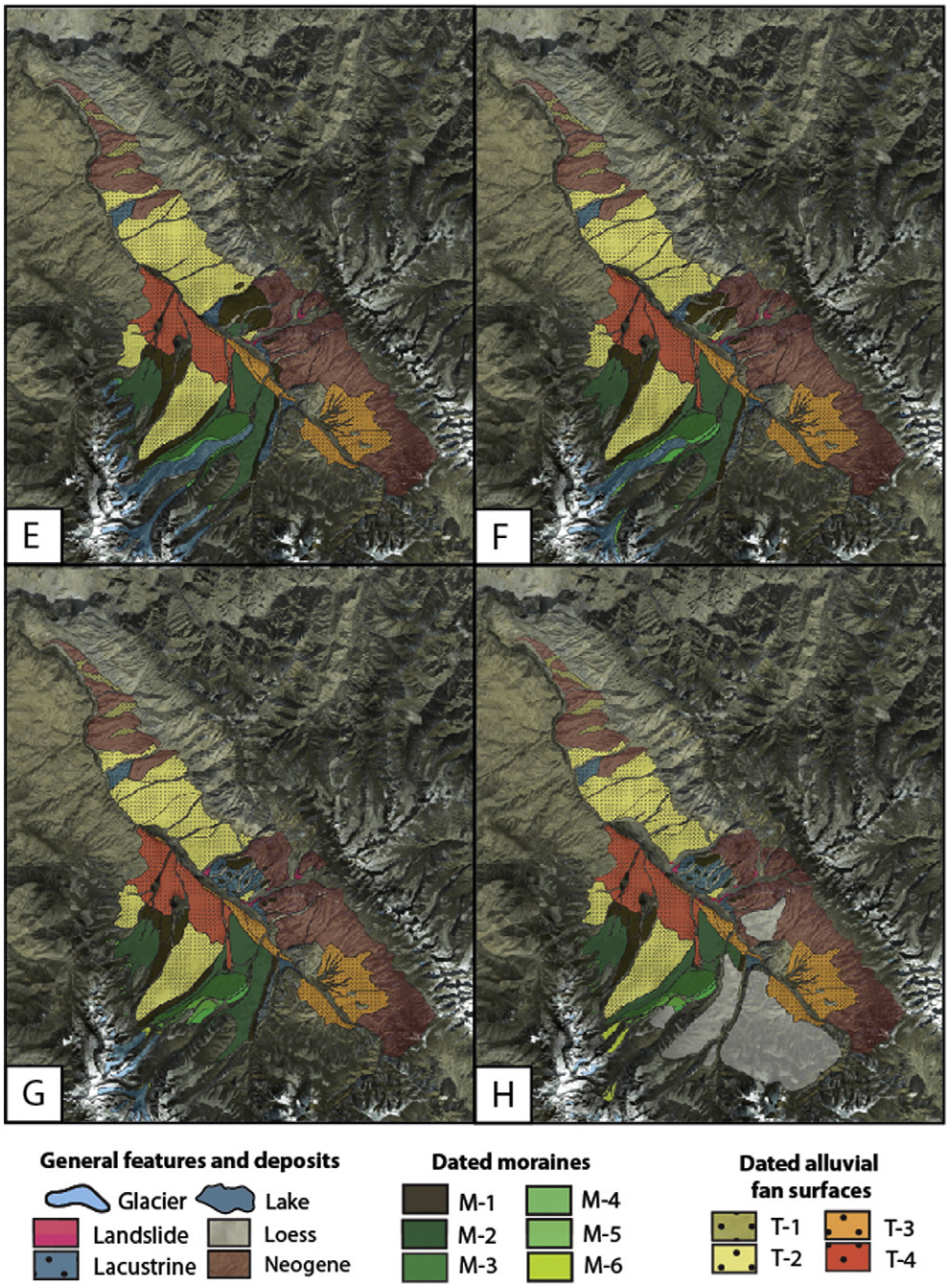

Fig. 11 (*continued*).

deep incision through the M-1 and M-2 glacial deposits upvalley and the fluvial and lacustrine deposits downvalley, resulting in the truncation of the T-2 alluvial fans.

Continued, more restricted glacial advances resulted in the deposition of another distinctive set of ground moraines (M-3; Fig. 11D) as fluvial erosion continued to remove older glacial deposits. This incision and erosion along the main Waqia River continued through the M-4 (~15 ka), M-5 (~10 ka), and M-6 (~10 ka) glacial advances. Glacial advances after M-3 were progressively more restricted in extent. The M-4 glacial advance was constrained by M-3 and older deposits (Fig. 11E). The M-5 glacial advance extended nearly as far as the M-4 advance but did not deposit as much sediment (Fig. 11F). The M-6 moraines are located far upvalley and were formed during continued retreat of glaciers in the Waqia valley (Fig. 11G).

Today, the Waqia River is eroding a broad channel bordered by sparse, thin fluvial terraces. Incision is >200 m from the top of T-2 to the present valley floor. Smaller, undated terraces are present along the upper Waqia valley floor. Most modern tributary streams, with the exception of glacially fed tributaries, are ephemeral and are braided within a narrow, entrenched channel. These tributaries typically do not reach the modern Waqia River channel and instead form broad alluvial/outwash fans at the tributary valley mouth which, in the upper Waqia valley, contribute to a thin (~25 m) bajada along the truncated base of the T-2 alluvial fans. This suggests that erosion and deposition at this time is limited.

Many landforms, deposits, and features are highly localized; glaciation and glacial deposits are restricted primarily to the SW side of the upper Waqia valley, whereas alluvial fans are preserved almost

exclusively along the valley's eastern range. Erosion of degraded lacustrine sediments beneath the former M-1 glacial extent (near location 8, Fig.2) and at the mouth of a glaciated tributary in the lower Waqia valley (location 1, Fig. 2) has resulted in erosive patterns typical in badlands topography and unique to those two locations in the field area. The southern extremes of the Waqia valley are draped in irregular deposits of loess up to 2 m thick, whereas outside of these regions loess cover is <30 cm or absent.

This proposed sequence of events suggests an environment with progressively lessened capacity for erosion because of a geomorphic change (disequilibrium as a consequence of lake drainage and resulting base level drop returning to equilibrium over time) and/or a climatic change (lowered precipitation), as evidenced by deep valley incision and entrenched tributaries that no longer reach the main river channel. This explanation also implies that there is potential for long periods of general landform stability (~500 ka, e.g., establishment of the T-1 to lake drainage at ~100 ka) interrupted by relatively brief periods of rapid and significant change (glaciation and erosion/incision from ~80 to 20 ka). Moreover, a strong spatial control on landscape evolution is evident. We suggest that this study highlights that in Himalayan-Tibetan valleys landscape evolution is punctuated in time and strongly controlled by climate.

7. Conclusion

The Quaternary evolution of the Waqia valley is complex, involving the interplay among glaciation, landsliding, lake formation, alluvial fan and river terrace formation, and erosion, which vary temporally and spatially. Using ^{10}Be methods, we dated six sets of moraines (M-1 to M-6) and four surfaces on alluvial fan and river terrace (T-1 to T-4). Moraine M-1 dates to the penultimate or older glacial cycle, M-2 to the early last glacial or older, but most probably late in the penultimate glacial cycle, M-3 to early last glacial, probably MIS 4, M-4 to MIS 2 possibly global LGM, M-5 to the Late Glacial, and M-6 to the early Holocene. Numerous younger moraines are also present but are very restricted and were not dated. These ages tentatively correlate with the Dabudaer (M-1 and M-2), Tashkurgan (M-3), and Kuzigun (M-4) glacial stages of Tashkurgan valley (Owen et al., 2012). We define the ages of four terraces to ~580 ka (T-1), ~120 ka (T-2), and early Last Glacial (possibly ~100 and ~70 ka for T-3 and T-4, respectively).

Our interpretation, though tentative, suggests dramatically different stages in Quaternary valley evolution with regards to the sedimentary landscape, some of which may coincide with climatic change: (i) the presence of Paleolake Waqia is characterized by a stage of lacustrine and fluvial deposition including T-2 (~103–208 ka) during MIS 6; (ii) glacial advance, possibly beginning in MIS 6/older and late MIS 6 form M-1 and M-2 landforms and deposits, respectively; (iii) drainage of Paleolake Waqia between ~100 and 60 ka (MIS 4) triggers erosion and incision of the main Waqia River and the creation of T-3 and T-4 terraces; (iv) significant erosion and river incision of both main Waqia River and tributaries because of lowered base level from Paleolake Waqia drainage through MIS 3; (v) glaciation in MIS 4 and 2 (M-3 and M-4, ~15 ka); and (vi) greatly restricted glaciation continues into the Holocene (M-5 and M-6).

The formation of Paleolake Waqia exhibited a lasting and profound influence on the basin's evolution, from deposition of thick (>100 m) beds of lacustrine sediments to its drainage, which influenced the timing and pattern of basin erosion. Remaining questions about the timing of lake drainage and the ages of and relationships among lacustrine deposits, older moraine, and alluvial fan surfaces might help resolve questions about the true rate at which this landscape has changed. The new glacial chronology data we provide are not well defined enough to attribute definitively to precise climatic events, but it is important for providing a first order framework on the rates and magnitudes of landscape evolution in this region.

Acknowledgements

We would like to thank Jason Dortch for use of his Matlab code for PDF determination. Many thanks for the two anonymous reviewers who provided very constructive comments on our manuscript helping to improve our contribution, and to the Editor for the very careful editorial review. The National Science Foundation for funding this research (EAR-0910759). MWC acknowledges support from the National Science Foundation (EAR-1153689). This research was also supported by the International Science and Technology Cooperation Program of China (2008DFA20860), and the grant from State Key Laboratory of Earthquake Dynamics of China (no. LED2010A04).

Appendix A. Supplementary data

Supplementary data to this article can be found online at http://dx.doi.org/10.1016/j.geomorph.2016.09.002.

References

Aoki, T., Imamura, M., 1999. Reconstructing the glacial chronology based on the ^{10}Be exposure age in the Khumbu Glacier, Eastern Nepal Himalaya. Proceedings of the Korea-Japan/Japan-Korea Geomorphological Conference, pp. 134–135.
Balco, G., Stone, J.O., Lifton, N.A., Dunai, T.J., 2008. A complete and easily accessible means of calculating surface exposure ages or erosion rates from ^{10}Be and ^{26}Al measurements. Quat. Geochronol. 8, 174–195.
Barnard, P.L., Owen, L.A., Finkel, R.C., 2006. Quaternary fans and terraces in the Khumbu Himalaya, south of Mt. Everest: their characteristics, age and formation. J. Geol. Soc. Lond. 163, 383–400.
Benn, D.I., Owen, L.A., 2002. Himalayan glacial sedimentary environments: a framework for reconstructing and dating former glacial extents in high mountain regions. Quat. Int. 97 (98), 3–26.
Blöthe, J.H., Munack, H., Korup, O., Fülling, A., Garzanti, E., Resentini, A., Kubik, P.W., 2014. Late quaternary valley infill and dissection in the Indus River, western Tibetan Plateau margin. Quat. Sci. Rev. 94, 102–119.
Braucher, R., Merchel, S., Borgomano, J., Bourlès, D.L., 2011. Production of cosmogenic radionuclides at great depth: a multi element approach. Earth Planet. Sci. Lett. 309 (1), 1–9.
Brown, E.T., Bendick, R., Bourles, D.L., Gaur, V., Molnar, P., Raisbeck, G.M., Yiou, F., 2002. Slip rates of the Karakoram fault, Ladakh, India, determined determined using cosmic ray exposure dating of debris flows and moraines. J. Geophys. Res. 107 (B9, 2192), 7-1–7-8.
Brunel, M., Arnaud, N., Tapponnier, P., Pan, Y., Wang, Y., 1994. Kongur Shan normal fault: type example of mountain building assisted by extension (Karakoram fault, eastern Pamir). Geology 22, 707–710.
Chevalier, M.-L., Hilley, G., Tapponnier, P., Van DerWoerd, J., Liu-Zeng, J., Finkel, R.C., Ryerson, F.J., Li Haibing, L., Liu, X., 2011. Constraints on the late Quaternary glaciations in Tibet from cosmogenic exposure ages of moraine surfaces. Quat. Sci. Rev. 30, 528–554.
Derbyshire, E., 1983. The Lushan dilemma: Pleistocene glaciation south of the ChangJiang (Yangste River). Z. Geomorphol. 27, 445–471.
Desilets, D., Zreda, M., 2006. Elevation dependence of cosmogenic ^{36}Cl production in Hawaiian lava flows. Earth Planet. Sci. Lett. 246, 277–287.
Dortch, J.M., Owen, L.A., Haneberg, W.C., Caffee, M.W., Dietsch, C., Kamp, U., 2009. Nature and timing of mega-landslides in northern India. Quat. Sci. Rev. 28, 1037–1056.
Dortch, J.M., Owen, L.A., Caffee, M.W., 2010. Quaternary glaciation in the Nubra and Shyok valley confluence, northernmost Ladakh, India. Quat. Res. 74, 132–144.
Dortch, J.M., Owen, L.A., Caffee, M.W., 2013. Timing and climatic drivers for glaciation across semi-arid western Himalayan-Tibetan orogen. Quat. Sci. Rev. (in revision).
Dunai, T.J., 2000. Scaling factors for production rates of in situ produced cosmogenic nuclides: a critical reevaluation. Earth Planet. Sci. Lett. 176, 157–169.
Fort, M., Peulvast, J., 1995. Catastrophic mass-movements and morphogenesis in the Peri–Tibetan ranges: examples for West Kunlun, East Pamir and Ladakh. In: Slaymaker, O. (Ed.), Steepland Geomorphology, pp. 171–198.
Hallet, B., Putkonen, J., 1994. Surface dating of dynamic landforms: young boulders on aging moraines. Science 265, 937–940.
Hewitt, K., 1999. Quaternary moraines vs catastrophic avalanches in the Karakoram Himalaya, northern Pakistan. Quat. Res. 51, 220–237.
Heyman, J., Stroeven, A., Harbor, J., Caffee, M.W., 2011. Too young or too old: evaluating 884 cosmogenic exposure dating based on an analysis of compiled boulder exposure 885 ages. Earth Planet. Sci. Lett. 302, 71–80.
Hidy, A.J., Gosse, J.C., Pederson, J.L., Mattern, J.P., Finkel, R.C., 2010. A geologically constrained Monte Carlo approach to modeling exposure ages from profiles of cosmogenic nuclides: an example from Lees Ferry, Arizona. Geochem. Geophys. Geosyst. 11. http://dx.doi.org/10.1029/2010GC003084 (18 pp).
Hughes, P.D., 2010. Geomoprhology and Quaternary stratigraphy: the roles of morpho-, litho- and allostratigraphy. Geomorphology 123, 189–199.
Imrecke, D.B., 2013. Tectonic Evolution of the Southeast Pamir (Unpublished doctoral thesis) University of Houston, Houston.

Kohl, C.P., Nishiizumi, K., 1992. Chemical isolation of quartz for measurement of in situ produced cosmogenic nuclides. Geochim. Cosmochim. Acta 56, 3583–3587.
Lal, D., 1991. Cosmic ray labeling of erosion surfaces: in situ nuclide production rates and erosion models. Earth Planet. Sci. Lett. 104, 429–439.
Lifton, N.A., Bieber, J.W., Clem, J.M., Duldig, M.L., Evenson, P., Humble, J.E., Pyle, R., 2005. Addressing solar modulation and long-term uncertainties in scaling secondary cosmic rays for in situ cosmogenic nuclide applications. Earth Planet. Sci. Lett. 239, 140–161.
Lifton, N., Sato, T., Dunai, T.J., 2014. Scaling in situ cosmogenic nuclide production rates using analytical approximations to atmospheric cosmic-ray fluxes. Earth Planet. Sci. Lett. 386, 149–160.
Martinson, D.G., Pisias, N.G., Hays, J.D., Imbrie, J., Moore, T.C., Shackleton, N.J., 1987. Age dating and the orbital theory of the ice ages: development of a high resolution 0–300,000-year chronostratigraphy. Quat. Res. 27, 1–29.
McDougall, I., Harrison, T.M., 1999. Geochronology and Thermochronology by the $^{40}Ar/^{39}Ar$ Method. second ed. Oxford University Press, Oxford, p. 269.
Murari, M.K., Owen, L.A., Dortch, J.M., Caffee, M.W., Dietsch, C., Fuchs, M., Haneberg, W.C., Sharma, M.C., Townsend-Small, A., 2014. Timing and climatic drivers for glaciation across monsoon-influenced regions of the Himalayan-Tibetan orogen. Quat. Sci. Rev. 88C, 159–182.
Owen, L.A., 1989. Terraces, uplift and climate in the Karakoram Mountains, Northern Pakistan: Karakoram intermontane basin evolution. Z. Geomorphol. 76, 117–146.
Owen, L.A., 1991. Mass movement deposits in the Karakoram Mountains: their sedimentary characteristics, recognition and role in Karakoram landform evolution. Z. Geomorphol. 35 (4), 401–424.
Owen, L.A., Derbyshire, E., 1993. Quaternary and Holocene intermontane basin sedimentation in the Karakoram Mountains. In: Shroder, J.F. (Ed.), Himalaya to the Sea: Geology, Geomorphology and the Quaternary. Routledge, London, pp. 108–131.
Owen, L.A., Dortch, J.M., 2014. Quaternary glaciation of the Himalayan-Tibetan orogen. Quat. Sci. Rev. 88, 14–54.
Owen, L.A., Finkel, R.C., Caffee, M.W., Gualtieri, L., 2002. Timing of multiple glaciations during the Late Quaternary in the Hunza Valley, Karakoram Mountains, Northern Pakistan: defined by cosmogenic radionuclide dating of moraines. Geol. Soc. Am. Bull. 114, 593–604.
Owen, L.A., Finkel, R.C., Ma, H., Spencer, J.Q., Derbyshire, E., Barnard, P.L., Caffee, M.W., 2003a. Timing and style of Late Quaternary glaciations in NE Tibet. Geol. Soc. Am. Bull. 11, 1356–1364.
Owen, L.A., Spencer, J.Q., Ma, H., Barnard, P.L., Derbyshire, E., Finkel, R.C., Caffee, M.W., Nian, Z.Y., 2003b. Timing of Late Quaternary glaciation along the southwestern slopes of the Qilian Shan. Boreas 32, 281–291.
Owen, L.A., Finkel, R.C., Barnard, P.L., Ma, H., Asahi, K., Caffee, M.W., Derbyshire, E., 2005. Climatic and topographic controls on the style and timing of Late Quaternary glaciation throughout Tibet and the Himalaya defined by ^{10}Be cosmogenic radionuclide surface exposure dating. Quat. Sci. Rev. 24, 1391–1411.
Owen, L.A., Caffee, M., Bovard, K., Finkel, R.C., Sharma, M., 2006a. Terrestrial cosmogenic surface exposure dating of the oldest glacial successions in the Himalayan orogen. Geol. Soc. Am. Bull. 118, 383–392.
Owen, L.A., Finkel, R.C., Ma, H., Barnard, P.L., 2006b. Late Quaternary landscape evolution in the Kunlun Mountains and Qaidam Basin, Northern Tibet: a framework for examining the links between glaciation, lake level changes and alluvial fan formation. Quat. Int. 154-155, 73–86.
Owen, L.A., Caffee, M.W., Finkel, R.C., Seong, B.S., 2008. Quaternary glaciation of the Himalayan–Tibetan orogen. J. Quat. Sci. 23, 513–532.
Owen, L.A., Robinson, R., Benn, D.I., Finkel, R.C., Davis, N.K., Yi, C., Putkonen, J., Li, D., Murray, A.S., 2009. Quaternary glaciation of Mount Everest. Quat. Sci. Rev. 28, 1412–1433.
Owen, L.A., Yi, C., Finkel, R.C., Davis, N., 2010. Quaternary glaciation of Gurla Mandata (Naimon'anyi). Quat. Sci. Rev. 29, 1817–1830.
Owen, L.A., Chen, J., Hedrick, K.A., Caffee, M.W., Robinson, A., Schoenbohm, L.M., Zhaode, Y., Li, W., Imrecke, D., Liu, J., 2012. Quaternary glaciation of the Tashkurgan Valley, Southeast Pamir. Quat. Sci. Rev. 47, 56–72.
Pigati, J.S., Lifton, N.A., 2004. Geomagnetic effects on time-integrated cosmogenic nuclide production with emphasis on in situ ^{14}C and ^{10}Be. Earth Planet. Sci. Lett. 226, 193–205.
Powell, R., Hergt, J., Woodhead, J., 2002. Improving isochron calculations with robust statistics and the bootstrap. Chem. Geol. 185 (3), 191–204.
Putkonen, J., O'Neal, M.A., 2006. Degradation of unconsolidated Quaternary landforms in the western North America. Geomorphology 75, 408–419.
Putkonen, J., Swanson, T., 2003. Accuracy of cosmogenic ages for moraines. Quat. Res. 59, 255–261.
Putkonen, J., Connolly, J., Orloff, T., 2008. Landscape evolution degrades the geologic signature of past glaciations. Geomorphology 97, 208–217.
Robinson, A.C., 2009. Evidence against quaternary slip on the northern Karakorum Fault suggests kinematic reorganization at the western end of the Himalayan-Tibetan orogen. Earth Planet. Sci. Lett. 286, 158–170.
Robinson, A.C., Yin, A., Manning, C.E., Harrison, T.M., Zhang, S.H., Wang, X.F., 2004. Tectonic evolution of the north eastern Pamir: constraints from the portion of the Cenozoic Kongur Shan extensional system, western China. Geol. Soc. Am. Bull. 116, 953–973.
Robinson, A.C., Yin, A., Manning, C.E., Harrison, T.M., Zhang, S.H., Wang, X.F., 2007. Cenozoic evolution of the eastern Pamir: implications for strain accommodation mechanisms at the western end of the HimalayaneTibetan orogen. Geol. Soc. Am. Bull. 119, 882–896.
Rodés, Á., Pallàs, R., Braucher, R., Moreno, X., Masana, E., Bourlés, D.L., 2011. Effect of density uncertainties in cosmogenic ^{10}Be depth-profiles: dating a cemented Pleistocene alluvial fan (Carboneras Fault, SE Iberia). Quat. Geochronol. 6 (2), 186–194.
Schäfer, J.M., 2000. Reconstruction of landscape evolution and continental paleoglaciations using in-situ cosmogenic nuclides: examples from Antarctica and the Tibetan Plateau. Diss. ETH Zürich. Der Andere Verlag, Osnabrück.
Scherler, D., Munack, H., Mey, J., Eugster, P., Wittmann, H., Codilean, A.T., Kubik, P., Strecker, M.R., 2014. Ice dams, outburst floods, and glacial incision at the western margin of the Tibetan plateau: a >100 k.y. chronology from the Shyok Valley, Karakoram. Geol. Soc. Am. Bull. 126, 738–758.
Seong, Y.B., Owen, L.A., Bishop, M.P., Bush, A., Clendon, P., Copland, P., Finkel, R.C., Kamp, U., Shroder, J.F., 2007. Quaternary glacial history of the Central Karakoram. Quat. Sci. Rev. 26, 3384–3405.
Seong, Y.B., Owen, L.A., Yi, C., Finkel, R.C., 2009a. Quaternary glaciation of Muztag Ata and Kongur Shan: evidence for glacier response to rapid climate changes throughout the Late Glacial and Holocene in westernmost Tibet. Geol. Soc. Am. Bull. 121, 348–365.
Seong, Y.B., Owen, L.A., Yi, C., Finkel, R.C., Schoenbohm, L., 2009b. Geomorphology of anomalously high glaciated mountains at the northwestern end of Tibet: Muztag Ata and Kongur Shan. Geomorphology 103, 227–250.
Staiger, J., Gosse, J., Toracinta, R., Oglesby, B., Fastook, J., Johnson, J.V., 2007. Atmospheric scaling of cosmogenic nuclide production: climate effect. J. Geophys. Res. 112, B02205. http://dx.doi.org/10.1029/2005JB003811.
Stone, J.O., 2000. Air pressure and cosmogenic isotope production. J. Geophys. Res. 105, 23753–23759.
Xu, X., Hu, G., Qiao, B., 2013. Last glacial maximum climate based on cosmogenic ^{10}Be exposure ages and glacier modeling for the head of Tashkurgan Valley, northwest Tibetan Plateau. Quat. Sci. Rev. 80, 91–101.
Yuan, Z., Chen, J., Owen, L.A., Hedrick, K.A., Caffee, M.W., Li, W., Schoenbohm, L.M., Robinson, A.C., 2013. Nature and timing of large landslides within an active orogen, eastern Pamir, China. Geomorphology 182, 49–65.